*Published online 30 January 2019* *Nucleic Acids Research, 2019, Vol. 47, No. 5* **2455–2471**
*doi: 10.1093/nar/gkz052*

# Dysregulation of the cohesin subunit RAD21 by Hepatitis C virus mediates host–virus interactions

**Shira Perez[1,2,†], Michael Gevor[1,3,†], Ateret Davidovich[1,†], Antony Kaspi[4], Katreena Yamin[3], Tom Domovich[1], Tomer Meirson[5], Avi Matityahu[3], Yehuda Brody[6], Salomon M. Stemmer[7], Assam El-Osta[4,8], Izhak Haviv[2], Itay Onn[3,*] and Meital Gal-Tanamy[1,*]**

[1]Molecular Virology Lab, Azrieli Faculty of Medicine, Bar-Ilan University, Safed, Israel, [2]Cancer Personalized Medicine and Diagnostic Genomics Lab, Azrieli Faculty of Medicine, Bar-Ilan University, Safed, Israel, [3]Chromosome Instability and Dynamics Lab, Azrieli Faculty of Medicine, Bar-Ilan University, Safed, Israel, [4]Epigenetics in Human Health and Disease Laboratory, Department of Diabetes, Central Clinical School, Monash University, Melbourne, Australia, [5]Cell Migration and Invasion Laboratory, Azrieli Faculty of Medicine in the Galilee, Bar-Ilan University, Safed, Israel, [6]The Broad institute of Harvard and MIT, Cambridge, MA, USA, [7]Davidoff Center, Rabin Medical Center, Beilinson Campus, Petach Tikva, and Sackler Faculty of Medicine, Tel Aviv University, Tel Aviv, Israel and [8]Hong Kong Institute of Diabetes and Obesity, Prince of Wales Hospital, The Chinese University of Hong Kong, Hong Kong SAR

Received May 02, 2018; Revised December 30, 2018; Editorial Decision January 18, 2019; Accepted January 24, 2019

## ABSTRACT

**Hepatitis C virus (HCV) infection is the leading cause of chronic hepatitis, which often results in liver fibrosis, cirrhosis and hepatocellular carcinoma (HCC). HCV possesses an RNA genome and its replication is confined to the cytoplasm. Yet, infection with HCV leads to global changes in gene expression, and chromosomal instability (CIN) in the host cell. The mechanisms by which the cytoplasmic virus affects these nuclear processes are elusive. Here, we show that HCV modulates the function of the Structural Maintenance of Chromosome (SMC) protein complex, cohesin, which tethers remote regions of chromatin. We demonstrate that infection of hepatoma cells with HCV leads to up regulation of the expression of the RAD21 cohesin subunit and changes cohesin residency on the chromatin. These changes regulate the expression of genes associated with virus-induced pathways. Furthermore, siRNA down-regulation of viral-induced RAD21 reduces HCV infection. During mitosis, HCV infection induces hyper-condensation of chromosomes and the appearance of multi-centrosomes. We provide evidence that the underlying mechanism involves the viral NS3/4 protease and the cohesin regulator, WAPL. Altogether, our results provide the first evidence that HCV induces changes in gene expression and chromosome structure of infected cells by modulating cohesin.**

## INTRODUCTION

Hepatitis C Virus (HCV) is an RNA virus with an exclusively cytoplasmic life cycle that infects human liver cells. HCV raises particular concern because of its ability to establish a chronic infection and its role in hepatocellular carcinoma (HCC), a challenging malignancy of global importance with increasing incidence over the past decades (1,2). Infection of liver cells by HCV has been shown to modify fundamental cell processes that affect the host genome, including its chromosomal stability (3). Infected cells are delayed in the G2/M phase of the cell cycle (4). In addition, HCV inhibits mitotic checkpoints and DNA repair, leading to a high frequency of polyploidy. These cellular changes have been suggested as a driving force for HCC (5–8). However, the mechanism by which the exclusively cytoplasmic virus affects nuclear processes and induces chromosomal instability (CIN) is not fully understood.

The HCV RNA encodes a polyprotein that undergoes proteolytic cleavage to generate four structural proteins (C, E1, E2 and P7) and six non-structural proteins (NS2, NS3, NS4A, NS4B, NS5A and NS5B). NS3 and its co-factor NS4A (NS3/4A) form a multi-functional protein containing a protease, and RNA helicase activity (9). The protease activity of NS3/4A is essential for the cleavage of the viral polyprotein. However, it has been shown that NS3/4A also cleaves cellular proteins as part of the viral mechanism of hijacking the cellular machinery (10–14). The preferred cleavage sequence of NS3/4 is cysteine or threonine followed by a serine (14). However, the sequence preferences of the protease are promiscuous and therefore, additional unidenti-

*To whom correspondence should be addressed.Tel: +972 72 2644 983; Fax: +972 72 2644 983; Email: Itay.Onn@biu.ac.il
Correspondence may also be addressed to Meital Gal-Tanamy. Tel: +972 72 2644 981; Fax: +972 72 2644 981; Email: Meital.Tanamy@biu.ac.il
†The authors wish it to be known that, in their opinion, the first three authors should be regarded as Joint First Authors.

fied cellular proteins may serve as NS3/4A cleavage targets (14).

The evolutionarily conserved Structural Maintenance of Chromosome (SMC) protein complex, cohesin, is important for faithful segregation of the sister chromatids during mitosis, chromosome condensation, and regulation of gene expression (15–17). Cohesin tethers together distinct regions of chromatin, and plays a central role in spatial organization of the genome (15,17,18). Mutations in genes encoding the cohesin subunits are associated with genetic disorders and cancer (19). Cohesin is composed of three core subunits, SMC1, SMC3 and RAD21 that form a heterotrimer. Another three proteins, SA/SCC3, WAPL and PDS5 form a subcomplex that interacts with the core subunits through RAD21 (17).

The regulatory subunit, WAPL, functions as a cohesin releasing factor that plays key roles in cohesin turnover on chromatin. Depletion of WAPL leads to prometaphase delay and an increase in the fraction of chromatin-associated cohesin (20–23). In WAPL depleted MEF cells, cohesin relocalizes and accumulates at sites of convergent transcription (23,24). These spatial changes in cohesin in WAPL depleted cells lead to hyper-condensation of interphase (vermicelli) chromatin, which is the result of unregulated extension of chromatin loops (22,23). To date, there have been no reports of a biological process in which the levels of WAPL in the cell are modified.

Interaction between virus and host factors is a central and essential process in the life cycle of HCV and other viruses. Interplay between cohesin and viral proteins has been shown for several viruses. In the Herpes viridae family, cohesin binds regulatory elements on the virus genome, and regulates the switch between the latent and lytic life cycles of the virus (25,26). Similarly, cohesin has been shown to regulate expression of genes of post-integrated HIV (27). A major difference between these viruses and HCV is that the life cycle of the former viruses is nuclear, while HCV is solely cytoplasmatic. Yet, it has been shown that HCV infection is associated with activation of genes that are essential for the virus life cycle such as genes in the lipid metabolism pathway (28). In addition, HCV infection induces chromosome instability (CIN) in cells (5–8). Therefore, an intriguing possible mechanism by which HCV affects these host nuclear processes is through regulation of cohesin functions. To date, such interplay has not been reported.

Here, we describe an interaction between HCV and cohesin. Infection of cells with HCV leads to increased expression of the cohesin subunit RAD21, and to changes in cohesin chromosomal residency. These changes affect gene expression and the structure of mitotic chromosomes. We provide evidence that the underlying mechanism involves the viral protease, NS3/4A, and the cohesin regulator, WAPL. These findings elucidate the mechanism whereby HCV can usurp cellular processes, and provide a rationale for the induction of HCC in infected cells.

## MATERIALS AND METHODS

### Cell lines

Huh-7.5 cells (a generous gift from Charles Rice) and Huh7/FT3-7 cells (a generous gift from Stanley M. Lemon) were cultured as described previously (29). Nontransformed THLE-3 (ATCC® CRL-11233™) immortalized normal human liver cells were maintained in BEGM Bullet Kit (Lonza Catalog No. CC-3170) containing medium added with 5 ng/ml EGF, 70 ng/ml Phosphoethanolamine and 10% fetal bovine serum. The cells seeded on palates precoated with a mixture of 0.01 mg/ml fibronectin, 0.03 mg/ml bovine collagen type I and 0.01 mg/ml bovine serum albumin dissolved in BEBM medium.

### Primary Human Hepatocytes (PHH)

Fresh resected normal human liver tissue was obtained at the Rabin Medical center under protocols approved by the Rabin Medical Center Institutional Review Boards and in accordance with the ethical standards of the Helsinki Declaration. Liver tissue was dissociated and cells seeded on palates precoated with collagen. Cells were maintained in Leibovitz's L-15 medium supplemented with 26 mmol/l $NaHCO_3$, 4 μg/ml insulin, 1 μM hydrocortisone hemisuccinate, and 10% heat-inactivated FBS, as previously described (30).

### Virus

HJ3–5 virus (29) stocks were produced in Huh7/FT3-7 cells, and viral titers were determined by FFU assay in Huh7.5 cells, as described previously (29). For all experiments with infected cells, cells were infected with HJ3-5 chimeric virus at a MOI of 0.1–0.5. In all experiments with infected Huh7.5 cells, except for the dynamics experiment in Figure 1A and B, infected cells were passaged for 2 weeks until ∼100% of the cells were HCV positive, as previously described (31). We maintained high infection levels for two weeks, by adding 2% human serum to the culture medium as previously described (32,33). PHH cells were infected with infectious HCV HJ3-5 at high MOI (0.5–1) to ensure high efficiency of infection, as described previously (34). PHH cells were harvested after 1 week in culture, when most of the cells were infected.

### Treatments of HCV infected cells with DAA

For DAA treated cells, HCV infected cells (∼100% infected, generated as described above) were treated with 0.05 μM paritaprevir for 7 days. Following treatment, cells were immunostained by HCV-positive serum of infected subject and anti-human 488 Alexa fluor (Jackson) as secondary antibody to ensure there is no HCV infection. Infection was visualized under epifluorescent microscope.

### ChIP and ChIP-seq

100% HCV infected (generated as described above) and non-infected Huh7.5 cells were fixed with 1% formaldehyde to cross-link proteins to DNA. Cells were then lysed, and chromatin was fragmented by sonication (Covaris S220) to generate DNA fragments of 200–1000 bp. ChIP was carried out using 5 μg of either anti-RAD21 Ab (BETHYL) or 5 μg of specific antibody against H3K9Ac Abs (Milipore) or normal Rabbit IgG Ab as control (Milipore) and Magna ChIP

G kit (Milipore). Cross-links were reversed, and DNA purified. The purified DNA was then used for RT- PCR and next generation sequencing (NGS) using Illumina HiSeq 2500.

### Treatments of HCV infected cells with p300/CBP inhibitor C646

Huh7.5 cells were infected with HJ3-5 chimeric virus at a MOI of 0.1 and passaged for 2 weeks until ∼100% of the cells were HCV positive. Two weeks post infection, infected cells were treated with 10 μM of C646 (Medchem Express). Medium containing drugs was replaced every 48 h for 8 days. RNA was purified, and RAD21 expression was quantified by qPCR as described below.

### siRNA transfection of RAD21

RAD21 siRNA (sense GGUGAAAAUGGCAUUACG GTT; antisense CCGUAAUGCCAUUUUCACCTT) and negative control siRNA (sense CGUACGCGGAAUAC UUCGATT; antisense CGAAGUAUUCCGCGUACG TT) were purchased from IDT. Prior to transfection, $10^5$ cells were seeded in 24-well plates and incubated for 24 h. Cells were transfected with 6 μg of siRNA using Oligofectamine Reagent (Invitrogen) according to the manufacturer's instructions. Cells were infected with HJ3-5 chimeric virus at a MOI of 0.5 48 h following transfection. The cells were incubated for 48 h following infection, and the medium was collected to determine viral titer, as previously described (31). The cells were then harvested for evaluation of HCV RNA and RAD21 RNA levels by qPCR as described below.

### ChIP-seq bioinformatics analysis

Short sequence tags were quality trimmed, and sequences shorter than 35 nt were discarded. The sequences were aligned to the GRCh37 (hg19) reference genome using BWA (35). Duplicate alignments were removed. Peaks were generated for each sample using MACS (36) with an input sample as background. Peaks were merged, with any region covered by at least two sample-based peaks used for downstream differential analysis. Aligned reads within the consensus peak regions were counted using bedtools multicov (37) with a minimum alignment quality threshold of 20. Differential analysis was performed using edgeR (38).

### RNA-Seq

Total RNA from 100% HCV infected (generated as described above) and non-infected Huh7.5 cells was purified using the RNeasy Mini Kit (Qiagen). Next, 1 μg of total RNA was treated with the NEB Next poly (A) mRNA Magnetic Isolation Module (New England Biolabs). RNA-seq libraries were produced by using the NEBNext Ultra RNA Library Prep Kit for Illumina (New England Biolabs), and sequenced by Illumina HiSeq 2500.

### RNA-Seq bioinformatics analysis

Short sequence tags were quality trimmed, discarding sequences shorter than 35 nt. The sequences were aligned to the GRCh37 (hg19) reference genome using STAR (36). Aligned reads were counted using featureCounts (39), by means of the Ensemble Version 75 transcript database. Differential analysis was performed using edgeR (38).

### Pathway analysis

Using the RNA-Seq and RAD21 ChIP-Seq data we generated ranked lists of differentially modified genes (DMGs, for ChIP-seq signal at a vicinity of a specific gene) and differentially expressed genes (DEGs, for RNA-seq signal) (Ranked from most significant decrease to the most significant increase). The two gene lists were used for gene ontology (GO) analysis using the MetaCore database from Thomson Reuters (version 6.11, build 41105, GeneGo, Thomson Reuters, New York, NY, USA) (40) pathway analysis tool. This pathway analysis tool was used to perform gene network enrichment analysis from integration of RNA-seq and Rad21 ChIP-seq data. All genes that were identified as DMGs or DEGs were included in the analysis. The enrichment analysis consisted of matching gene IDs of possible targets for the 'common' (black/white bar), and 'unique' (RNA-seq-black, Rad21 ChIP-seq-grey) sets with gene IDs in functional ontologies in MetaCore. The probability of a random intersection between a set of IDs the size of the target list with ontology entities is estimated by the *P* value of the hypergeometric intersection. The lower *p* value reflects higher relevance of the entity to the dataset, which shows a higher rating for the entity. A canonical pathway represents a set of signaling and metabolic maps. These are created based on published peer reviewed literature using the Thompson Reuter MetaCore analysis, GeneGo. The top scored maps (map with the lowest *P* value) are based on the enrichment distribution sorted by the 'common' set.

### Quantitative RT-PCR

Total RNA from tested cells was extracted using a RNA kit (Qiagen). Equal amounts of the RNA isolated from treated or control cells were transcribed into cDNA using the High Capacity cDNA Reverse Transcriptase kit (Applied Biosystems) and analyzed by RT-PCR using Power SYBR Green Master Mix (Life Technologies). Oligonucleotides were designed using the Primer3 PCR Primer Design Tool according to the RNA-Seq and ChIP-seq data. The thermal program included a 10 min incubation at 95°C to activate the FastStart Taq polymerase, followed by 40 cycles of 95°C for 10 s, 58°C for 10 s and 72°C for 20 s. The fluorescence readings were recorded after each 72°C step. Dissociation curves were performed after each PCR run to ensure that a single PCR product had been amplified. Differential expression was calculated using the equation of $2^{(-\Delta\Delta Ct)}$, with the GAPDH as the endogenous controls. RT-PCR analysis using RNA from three independent experiments was conducted. For validation of ChIP-seq data, primers for qPCR were designed to target the peaks of the tested genes according to the RAD21 ChIP-Seq data**.** Purified DNA following ChIP with anti-RAD21 Ab was quantified by qPCR. Values were normalized relative to qPCR for these genes following ChIP with normal Rabbit IgG Ab as control. Real time quantitative RT-PCR was carried out using

primers for the 3′-untranslated region (UTR) of HCV: (FW GCCATGGCGTTAGTATGAGTGT; REV CCCTATCA GGCAGTACCACAA), and RAD21 (FW CCTCAGCA GGTAGAGCAAATGG; REV GCATCTGCTGAGTG CGTTTGTT). The primers for the detection of the acetylation state of RAD21 promoter by qPCR following H3K9Ac ChIP were designed to span the interval chr8:117886000-117887000: RAD21gDNA FW GGAGGAAAAGAAGG GGTCGG; RAD21gDNA REV CTGCTCGGAAGCTA CACCTC. Values were normalized relative to qPCR for these genes following ChIP with normal Rabbit IgG Ab as control.

### Cell cycle arrest

HCV infected (100% infected, generated as described above) and non-infected Huh7.5 cells were arrested at the G0/G1, G1/S and G2/M stage using 2% DMSO, 0.1 μg/ml hydroxyurea, or 0.3 μg/ml nocodazole, respectively. Cells were grown until they reached 90% confluence. For flow cytometry, cells were washed with 1× PBS and re-suspended in 1 ml, 70% cold EtOH. Prior to FACS assay, the cells were washed with 1× PBS and re-suspended in 100 μl of a solution containing 50 μg/ml propidium iodide and 1 mg/ml RNase in PBS for 2 h. The cell suspension was gently mixed and incubated at 37°C for 30 min, and 300 μl of PBS was added before proceeding to FACS assay. The cell cycle profiles were then analyzed using a Flow Cytometer (Galios). At least 10 000 cells in each sample were analyzed to obtain a measurable signal. All measurements were performed using the same instrument setting.

### Cell fractionation

Nuclear and cytoplasmic extracts were prepared from HCV infected and non-infected Huh7.5 cells as previously described (41), with some modifications. Briefly, $1 \times 10^7$ cells were pelleted and resuspended in 200 μl of Buffer A [10 mM HEPES–KOH pH 7.9, 1.5 mM $MgCl_2$, 10 mM KCl, 0.5 mM dithiothreitol, supplemented with protease inhibitor cocktail (Sigma)] and incubated on ice for 10 min. After centrifugation at 12 000 rpm for 30 s, cytoplasmic extract (supernatant) was harvested. The pellet was washed three times using 1 ml buffer A supplemented with 0.2% NP-40 to remove any residual cytoplasmic extracts and peri-nuclear proteins. The pellet was then resuspended in 50 μl buffer C (20 mM HEPES–KOH pH 7.9, 25% glycerol, 420 mM NaCl, 1.5 mM $MgCl_2$ and 0.2 mM EDTA) and protease inhibitor cocktail and incubated on ice for 1 h with intermittent vortexing at 4°C. After centrifugation at 12 000 rpm for 5 min, the supernatant was collected and used as a source of nuclear proteins. Both nuclear and cytosolic proteins were detected by western blot.

### Western blot

Nuclear and cytosolic fractions or total cell lysates were separated by SDS-PAGE. The proteins were transferred to nitrocellulose membranes and incubated with the primary antibodies RAD21 (BETHYL), Kap-1 (BETHYL) (nuclear fraction marker), and tubulin (SIGMA) (cytoplasmic fraction marker) as an internal control, and WAPL (Abcam). After removal of the unbound primary antibody, membranes were incubated with secondary antibody–peroxidase conjugate (Jackson), processed for detection by chemiluminescence (Advansta) and imaged on a ImageQuant LAS 4000. Protein levels were quantified and normalized to Kap-1 and tubulin using ImageJ software.

### Chromosome spread

For chromosome spreads, HCV infected (100% infected, generated as described above) and non-infected Huh7.5 cells or DAA treated cells (generated as described above) were used. For preparation of metaphase cells, nocodazole (final concentration 0.1 μg/ml) was added to the culture medium of the cells for 12 h before cell harvest. Mitotic cells were collected by quick trypsinization, and treated with 75 mM KCl at 37°C for 30 min. and then dropped onto coverslips. The chromosome spreads were fixed with methanol: glacial acetic acid (3:1) fixative solution, and incubated with DAPI. Wide field fluorescence images were obtained using the Zeiss AxioImager M2 system fully motorized upright microscope (100XPlan-Apo, 1.4N/A) driven by Zen blue software. The 3D images were deconvolved using a point spread function (PSF) based deconvolution algorithm Huygens Essential II (Scientific Volume Imaging, Hilversum, The Netherlands), and processed by Imaris (Bitplane).

### Multipolar spindle analysis

HCV infected (100% infected, generated as described above) and non-infected Huh7.5 cells were grown in 8-well glass chambers. Cells were arrested 8 days post infection in prometaphase by nocodazole. After synchronization, the medium was replaced to enable the cells to proceed to later stages of mitosis, and then processed for immunostaining. Immunofluorescence staining was carried out on paraformaldehyde-fixed cells. Cells were first permeabilized with a solution containing Triton X-100 0.5% and incubated overnight at 4°C with mouse anti-α tubulin antibody (Sigma-Aldrich) diluted 1:400 in PBS/1% BSA. After extensive washing, cells were incubated with Cy-3 conjugated anti-mouse antibody (Sigma-Aldrich) diluted 1:400 in PBS/1% BSA and mounted in Vectashield® Mounting Medium with DAPI (Vector Laboratories). Images were obtained on a Zen Apotome immunofluorescenece microscope (Zeiss).

### Transfection of HCV proteins

Expression plasmids pCDNA3.1-Hygro-NS4ANS3 and pCDNA3.1-Hygro-Core for the expression of NS4ANS3 or Core (a generous gift from Prof. Itai Benhar, Tel-Aviv University), were transfected into Huh7.5 or THLE-3 cells using polyethylenimine (PEI). In brief, 12 ng of the plasmids were mixed with 24 μl of PEI. Following vortex, the tubes were incubated for 10 min at room temperature. The mixtures were added to the cells and mixed followed by 24 h incubation. The medium was then replaced with DMEM. Following incubation for 48 h, cells were harvested for quantitative RT-PCR, chromosome spreads, or

multipolar spindle analysis as described above. Transfection efficiency was determined by Immunostaining with HCV-positive serum of infected subject and anti-human 488 Alexa fluor (Jackson) as secondary antibody.

### Analysis of HCC development in HCV infected patients

Microarray-based genome-wide profile data was obtained from the NCBI Gene Expression Omnibus (GSE15654) (42) using MATLAB (The Mathworks, Inc.). The dataset included gene expression profiles of liver biopsies from 216 patients with hepatitis C-related Child-Pugh class A cirrhosis. The log-rank test and Cox regression modeling were used to evaluate association between *RAD21* expression and time from the enrollment to development of HCC using R statistical package (www.r-project.org). Patient samples were split into high and low *RAD21* expressing groups based upon *Z*-score cutoff of 1.

### Superimposition of RAD21 HCV-altered binding sites on copy number variations (CNVs) in HCC

The RAD21 binding sites that are altered following HCV-infection identified by ChIP-seq were compared with a series of genomic intervals that encompass the boundaries of common copy number variations (CNVs) in HCC by GISTIC2 algorithm (43). The difference between the expected random overlap among cohesin genomic positioning and CNV boundaries was calculated using INRICH algorithm (44). Moreover, the list of genes associated with cohesin binding site that are changes in HCV infected cells was compared with a another list of 98 genes within intervals of CNVs detected in HCC (45). Statistical significance for the correlation was calculated by hypergeometric test.

## RESULTS

### HCV infection increases the expression of the cohesin subunit *RAD21* through activation of p300/CBP

The immediate effect of many viruses in infected cells is hijacking the transcription system, and its modulation for viral proliferation (28). As cohesin was identified as a regulator of gene expression, we evaluated the possibility that HCV misregulates cohesin levels in the cells. We infected Huh7.5 cells with the commonly used chimeric 1a/2a virus, HJ3-5, which replicates and produces infectious viruses (29). Cells were infected with HJ3-5 at an MOI of 0.1. Expression level of RAD21 and the dynamics of infection were determined by qPCR using primers for RAD21 and for the 3′ UTR of the viral genome, respectively. At four days post infection, expression of *RAD21* was increased by ∼2-fold compared to the uninfected control, and then declined (Figure 1A), concordantly with the peak of viral RNA replication (Figure 1B). To further validate that RAD21 is specifically upregulated in response to HCV infection we maintained the infected cells for 2 weeks to obtain a steady-state of viral infection which better simulates the state chronic infection. Then, we cured the infection with DAA. The results in Figure 1C demonstrate a twofold increase of RAD21 mRNA level in HCV-infected cells. However, RAD21 mRNA level was reverted to the level of control non-infected cells in HCV infected cells treated with DAA. DAA did not have any effect on RAD21 expression in non-infected cells (Figure 1C).

The experiments above were conducted in Huh7.5 cell line. To verify these results in primary cells, we infected normal primary human hepatocytes (PHH) with HCV. Similar to the results in Huh7.5 cells, we detected twofold increase in RAD21 expression compared with non-infected cells (Figure 1D and E). We concluded that HCV infection upregulates RAD21 gene expression.

We investigated the possibility that the change in RAD21 expression is mediated by HCV-induced epigenetic changes. The histone modification histone H3 acetylated on lysine 9 (H3K9Ac), that is an epigenetic marker for transcriptional activation, was previously associated with liver-specific epigenetics (46,47). Therefore, we evaluated whether the HCV-induced change in RAD21 expression correlates with an increased H3K9Ac level at the promoter of this gene. HCV infected Huh7.5 cells (100% infection for two weeks) were used for chromatin immunoprecipitation with antibody against H3K9Ac. The enrichment of RAD21 promotor was evaluated by qPCR. We found a twofold increase in acetylation in this region, suggesting that RAD21 expression is activated in response to HCV infection (Figure 1F). Inhibition of the histone acetyl transferase (HAT) p300/CBP, which mediates acetylation of H3K9, by its selective inhibitor C646 in infected cells partially restored RAD21 expression to its native levels, compared with non-infected C646 treated cells. We have recently found that treatment with C646 reduces HCV infection (unpublished data). Collectively, these results suggest a role for p300/CBP in RAD21 expression (Figure 1G).

We tested if the increased expression of the RAD21 gene is associated with increased levels of the protein. Surprisingly, we did not detect a significant change in the steady state levels of RAD21 in asynchronous cells when we analyzed total cell extracts by western blot with antibody against RAD21. As cohesin is temporally and spatially regulated (17), we explored whether the increased expression of the RAD21 gene may affect cohesin localization in the cell at different stages of the cell cycle. We arrested non-infected and infected Huh7.5 cells at the G0, S or G2/M stages of the cell cycle by supplementing the cell medium with DMSO, hydroxyurea, or nocodazole, respectively (Supplementary Figure S1). HCV infected and non-infected cells demonstrated similar profiles of cell cycle stages in both unsynchronized as well as in synchronized cells (Supplementary Figure S1). Whole cell extracts were prepared and fractionated to cytoplasmic and nuclear fractions using a sucrose cushion. Samples were analyzed by western blot with an antibody against RAD21. No significant difference in RAD21 levels was detected in the cytoplasmatic fraction in cells arrested at G0, S phase, or in prometaphase arrested cells (Figure 1H). Similar results were obtained in the nuclear fraction of G0 and S-phase arrested cells. However, a twofold increase in RAD21 levels was observed in the nuclear fraction of infected prometaphase cells, compared with non-infected cells at the same stage of the cell cycle (Figure 1H and I). These results suggest that nuclear RAD21 is increased in mitosis prior to chromosome segregation, and its dissolution is inhibited by HCV.

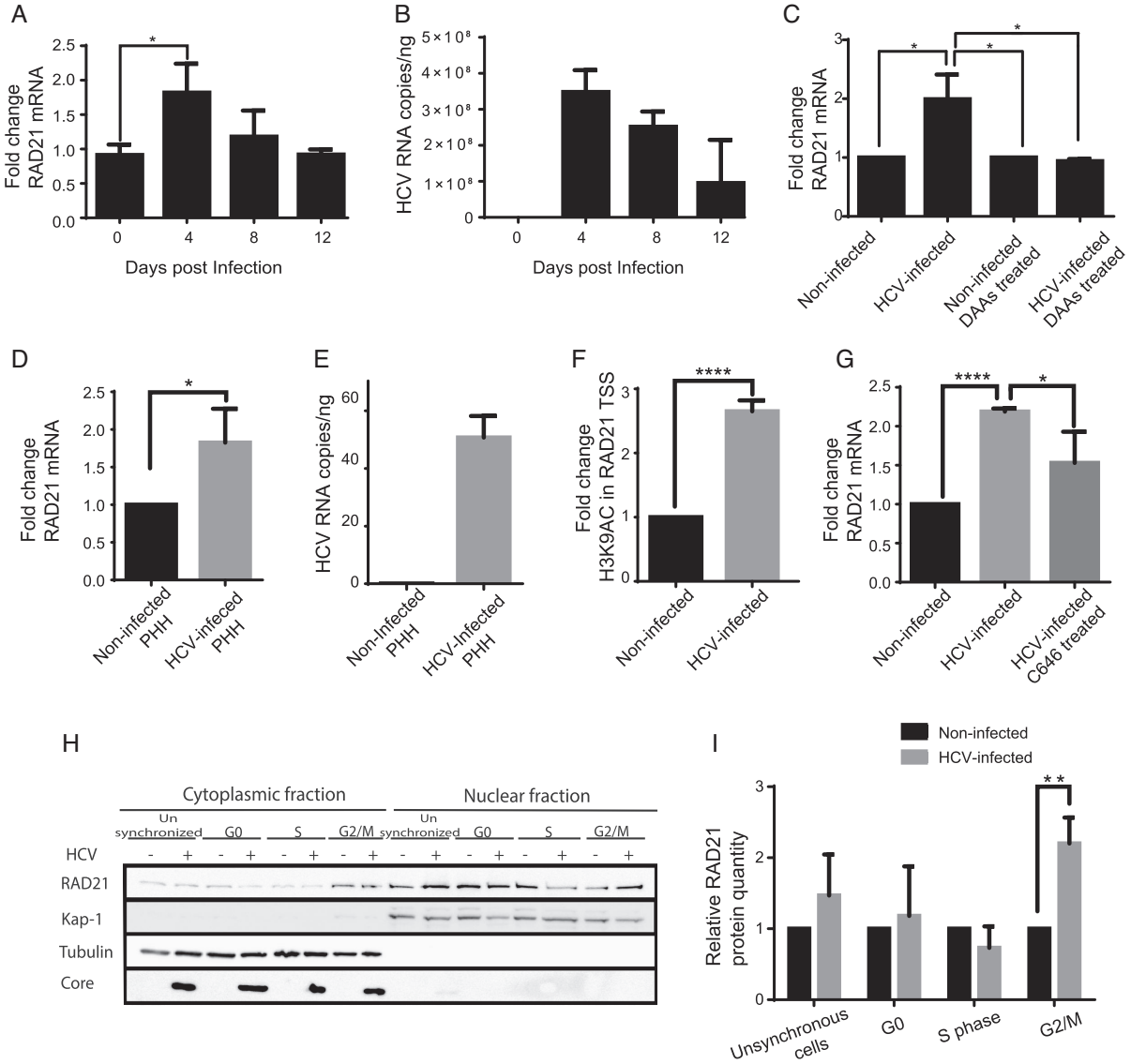


**Figure 1.** HCV infection increases the expression of cohesin. (**A**) Levels of mRNA of *RAD21* gene in HCV-infected Huh7.5 cells compared to control non-infected cells following 4, 8 and 12 days post infection evaluated by qRT-PCR. Fold change is calculated compared to non-infected Huh7.5 cells and presented as means fold change compared to control ± SD from three independent experiments (*$P = 0.0215$, *t*-test). (**B**) Levels of HCV RNA in HCV-infected Huh7.5 cells compared to control non-infected cells following 4, 8 and 12 days post infection evaluated by qRT-PCR. HCV RNA copies are calculated compared to non-infected Huh7.5 cells per ng of total cellular RNA. Data from three biological replicates are presented as means ± SD. (**C**) Levels of mRNA of *RAD21* gene in non-infected, HCV-infected, non-infected DAA treated and HCV-cured cells following treatment with DAA evaluated by qRT-PCR. Fold change is calculated compared to non-infected Huh7.5 cells and presented as means fold change compared to control ± SD from three independent experiments (*$P = 0.0215$, *t*-test). (**D**) Levels of mRNA of *RAD21* gene in HCV-infected PHH cells compared to control non-infected PHH cells evaluated by qRT-PCR. Fold change is calculated compared to non-infected PHH cells. Data from three biological replicates are presented as means ± SD (*$P = 0.04$, *t*-test). (**E**) Levels of HCV RNA in HCV-infected PHH cells compared to non-infected PHH cells evaluated by qRT-PCR. HCV RNA copies are calculated compared to non-infected PHH cells per ng of total cellular RNA. Data from three biological replicates are presented. (**F**) Enrichment of H3K9Ac in RAD21 transcription start site (TSS) evaluated in HCV infected Huh7.5 cells compared to non-infected cells following chromatin immunoprecipitation with antibody against H3K9Ac. The enrichment of RAD21 was evaluated by qPCR with primers specific to RAD21 TSS. Values were normalized relative to qPCR for these genes following ChIP with normal Rabbit IgG Ab as control. Data from three biological replicates are presented as means ± SD (**** $P < 0.0001$, *t*-test). (**G**) Levels of mRNA of *RAD21* gene in HCV-infected Huh7.5 cells compared to non-infected cells following C646 treatment evaluated by qRT-PCR. Fold change is calculated compared to non-infected Huh7.5 cells treated with C646 and presented as means ± SD from three biological replicates (**** $P < 0.0001$, * $P < 0.02$, *t*-test). For all qPCR experiments differential expression was calculated using the equation of $2^{(-\Delta\Delta Ct)}$, with the GAPDH as endogenous controls. (H and I) Relative quantity of RAD21 proteins at the nucleus at different stages of the cell cycle. Infected and non-infected Huh7.5 cells treated with DMSO (G0), hydroxyurea (S) and nocodazole (G2/M). Cells were lysed and fractionalized to cellular and nuclear extract. Protein levels of RAD21 were evaluated by Western blot (**H**). RAD21 protein levels were quantified from four biological replicates and normalized to Kap-1 and tubulin using the ImageJ software (**$P = 0.0046$, *t*-test) (**I**).

### HCV infection alters genome-wide cohesin binding, correlating with misregulation of gene expression

HCV has been shown to modulate the transcriptome of infected cells to support viral production (28). While the total amount of RAD21 on the chromatin was similar in uninfected and HCV-infected cells at interphase, we explored the possibility that HCV might modify the chromosomal residency of cohesin in order to affect gene expression. This possibility was tested by infecting Huh7.5 cells with HJ3-5 virus, and passaging the cells until ∼100% of the cells were positive for HCV. These cells were used for chromatin immunoprecipitation followed by next generation sequencing (ChIP-seq) of the RAD21 cohesin subunit. The analysis of differential peaks is presented in Figure 2A demonstrating the number of counts per million (CPM- the $\log_2$ of the read abundance determined by edgeR) for each peak versus the $\log_2$ fold change between infected and non-infected cells. Data revealed over 4400 RAD21 binding sites distributed along the genome with significant change in infected compared with non-infected cells (Figure 2A, red dots). Overall, we observed enrichment of RAD21 on the chromatin in infected cells (Figure 2A, red dots, $\log_2$ fold change $> 0$). Intersection of these data with annotated genomic features revealed that these binding sites are enriched mainly at regulatory elements including CpG islands, enhancers, and promoters (Figure 2B). This annotation defined the differentially modified genes (DMGs; genes in the vicinity of differential ChIP-seq peaks) induced by HCV infection for each ChIP-seq experiment.

In an attempt to correlate between cohesin relocalization in HCV infected cells and gene expression, we determined the changes in the transcriptome of HCV-infected compared to non-infected cells. Huh7.5 cells were infected with HCV as described above, and used for transcriptome profiling by RNA-seq. The analysis of differential peaks (HCV-infected compared to non-infected cells) identified 2672 differentially expressed genes (DEGs) when using a threshold of at least a 1.5-fold change in expression, with $P < 0.05$. The full description of these gene expression data will be reported elsewhere. We have generated a ranked list of DMGs (for ChIP-seq signal at a specific gene) and DEGs (for mRNA) (Ranked from most significant decrease to the most significant increase). Plotting the mRNA rank, indicating the difference in expression, against the differential ChIP-Seq ranks indicating RAD21 differential chromosomal residency, revealed a positive correlation (Figure 2C, Spearman rank: $P = 9.35e{-}17$). These results show that level of change in expression of genes following HCV infection is correlated with the level of change in RAD21 residency on the chromatin following HCV infection at the position of these same genes. Furthermore, this correlation was maintained when the mRNA rank was plotted against the differential residency of RAD21 at transcription start sites (TSS) (Figure 2D, Spearman rank: $P = 5.88e{-}12$). These results strongly indicate a positive association between cohesin chromosomal residency and gene expression changes in HCV infected cells.

To further investigate the signaling pathways that are disrupted by HCV infection due to misregulation of cohesin, we subjected the outlier RNA-Seq DEGs and RAD21 ChIP-Seq data to the Thompson Reuter MetaCore analysis pipeline, GeneGo. Several enriched pathways were found to be common in both RNA-seq and RAD21 ChIP-seq data. The full description of the pathways and their statistical significance is described in Supplementary Table S1. Among the top pathways are regulation of lipid metabolism, K-RAS signaling, HGF signaling, cytoskeleton remodeling and immune response (Figure 2E). These pathways are implicated in HCV lifecycle and pathogenesis (28,48). However, this is the first report that these expression changes correlate with cohesin residency. The scores of these pathways were evaluated by *P*-value for the enrichment of genes in these pathways common to RNA-seq and RAD21 ChIP-seq datasets. High statistical significance was found for the enrichment of these pathways in the common datasets ($0.00005 \leq P \leq 0.00158$). In contrast, the enrichment of genes in these pathways at sites of altered chromatin binding unique to the RAD21 ChIP-seq data was not significant ($P = 1$) (Figure 2E). This analysis supports the involvement of HCV-induced re-positioning of RAD21 on the chromatin in the regulation of these pathways through gene expression.

The enrichment of RAD21 on specific locations and the change in mRNA was validated by PCR on a panel of genes participating in these pathways. These genes are involved in cell proliferation, differentiation and survival (MUC20, INHBB, FGF21, RRAD,), cytoskeleton remodeling and invasion (SNAI1, FGF21, BAIAP2L2, lipid metabolism (FFAR2), inflammation (AMBP) and glucose metabolism (SLC2A10). The full description of the biological impact of the selected genes is provided in Supplementary Table S2. Overall, the qPCR gene-specific methods validated the up-regulation or down regulation signals we observed in the genome-wide analysis (Figure 2F, G and Supplementary Table S2). In most genes, increased or decreased RAD21 binding correlated with increase or decrease in gene expression, respectively. However, we observed also an opposite trend (MUC20, FFAR2 and SLC2A10). This observation is in agreement with the known effects of cohesin that may induce both activation or suppression of gene expression (49–51).

To validate that the change in enrichment of RAD21 levels in the promotors of these genes is HCV-specific, we performed RAD21-ChIP followed by qPCR to the tested genes also in HCV-cured cells following DAA treatment. The results show the reversion of RAD21 level in HCV-cured cells compared to HCV-infected cells for all tested genes (Figure 2H).

### Increased expression of RAD21 affects HCV infection

We showed that HCV infection increases cohesin expression and changes cohesin localization on chromatin in cells. Since these changes correlate with expression of genes involved in the HCV life cycle and oncogenesis, we tested the possibility that reducing RAD21 expression to its level in uninfected cells will also interfere with HCV infection. To this end, we partially depleted RAD21 from Huh7.5 cells by siRNA. To eliminate cell cycle effects of RAD21 depletion, the experiment was performed on non-dividing cells that were maintained in DMSO. In HCV infected Huh7.5 cells, RAD21 expression in RAD21 siRNA-treated cells was

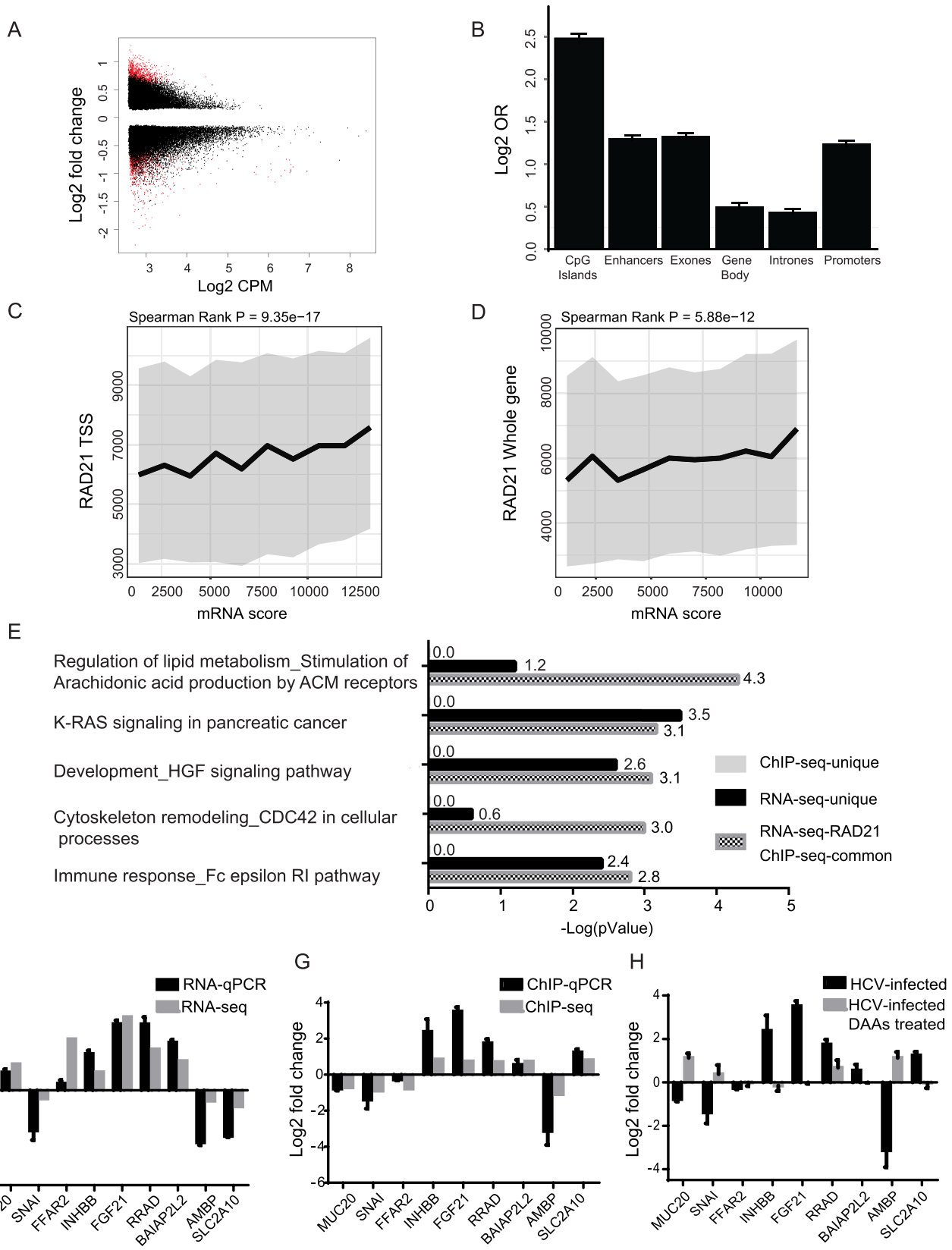


**Figure 2.** Integration of genome wide alteration in RAD21 chromosomal binding sites and gene expression following HCV infection. (**A**) Change in genome-wide distribution of RAD21 following HCV infection (100% HCV infected, generated as described in the methods) determined by RAD21 ChIP-seq experiment. The plots show the number of counts per million (CPM- the log2 of the read abundance determined by edgeR) for each peak versus the $\log_2$

60–80% lower compared to the control siRNA-treated cells (Figure 3A, B). Under these conditions, HCV infection, measured by HCV RNA level (Figure 3C) and virus titer (Figure 3D) was 40–60% lower in the RAD21 depleted cells compared with the control treated cells. As demonstrated in Supplementary Figure S2, the siRNA-mediated depletion of RAD21 has no effect on cellular viability. These changes in HCV production demonstrate that although RAD21 is not essential for HCV infection, HCV-induced RAD21 misregulation enhances HCV infection, and thus affects HCV life cycle.

### HCV induces chromosome hyper-condensation and the appearance of multi-polar spindles

In addition to its function in gene expression regulation, cohesin is a guardian of genomic stability (52). It has been shown that HCV induces CIN in the host cell by an unknown mechanism that eventually leads to HCC (5,53,54). The increased levels of cohesin in the nuclei of HCV-infected cells may induce structural changes in mitotic chromosomes. To explore the morphology of chromosomes following HCV infection, Huh7.5 cells were infected with HCV. When ∼100% of the cells were infected, cells were arrested at prometaphase by nocodazole treatment. Chromosomes from the infected and non-infected control cells were seeded, stained with DAPI and observed by fluorescence microscopy. Strikingly, we observed a hypercompacted morphology of chromosomes in the nuclei of infected cells (Figure 4A). This morphology was found in about 20% of the non-infected cells. However, hypercompacted chromosomes were observed in >80% of the HCV infected nuclei (Figure 4B). The NS3/4A protease can be specifically inhibited by the direct-acting antiviral (DAA) paritaprevir (55). The hypercondensation of the chromosome was therefore tested in uninfected and infected cells in the absence or presence of paritaprevir. Strikingly, treating the cells with NS3/4A inhibitor restored the normal condensation state of the chromosomes (Figure 4B). To better characterize the hypercompact chromosomes, we evaluated their physical properties. The average length of chromosomes from uninfected nuclei was >4 μm (Supplementary Figure S3A). In the infected nuclei, the chromosome length was shortened by 2-fold to ∼2 μm. The average volume and area of the chromosomes of infected nuclei were about 50% less than in uninfected nuclei (Supplementary Figure S3B and C). The measured DAPI staining intensity/$\mu m^3$ of chromosomes in infected nuclei was fourfold higher than in uninfected nuclei, indicating that the chromosomes of infected cells appear smaller due to hypercondensation (Figure 4C).

Recent reports suggested that RAD21 and cohesin have a role in centrosome integrity that is independent of its function in sister chromatid cohesion (56). We tested the possibility that HCV-induced misregulation of cohesin leads to centrosome abnormalities. Huh7.5 non-infected, HCV-infected (100% infection for two weeks), non-infected DAA treated and HCV-cured DAA treated cells were arrested in prometaphase by nocodazole. After synchronization, medium was replaced to enable the cells to proceed to later stages of mitosis, and the cells were then processed for immunostaining. Chromosomes were stained with DAPI while the spindles were immunostained with antibody against α-tubulin. Cells were also immunostained for viral proteins to verify infection. We observed a low background of approximately 4% of cells with multipolar spindles in non-infected cells, probably since Huh7.5 cells are derived from a hepatoma. Remarkably, we observed a twofold increase of multipolar spindle events in HCV-infected cells (Figure 4D and E), which reverted to the level of control non-infected cells following curing the infection with DAA. No effect of DAA on multipolar spindle formation has been found in non-infected cells (Figure 4D and E).

### The HCV-induced overexpression of RAD21 is associated with increased risk for HCC development.

We aimed to evaluate the potential effect of these observations on HCC development. To predict the effect of HCV-induced overexpression of RAD21, we analyzed Microarray-based genome-wide profile data obtained from the NCBI Gene Expression Omnibus (GSE15654) (42).

←

fold change between infected and non-infected cells for each peak. Regions subjected to significant changes are shown in red (adjusted $P$-value < 0.05), and non-significant changes are shown in black. Six biological replicates were performed for RAD21 ChIP-seq. (**B**) Over representation of all RAD21 peaks in genomic features (CpG islands, Enhancers, Exons, Promotors, Introns and gene body). Peaks were compared using a Fisher exact test to a background set which was generated by taking an equal sized random region within 1 Mbp of each RAD21 peak. The Y axis is the $\log_2$ Odds Ratio)OR(. The error bars are 95% confidence intervals. (**C** and **D**) Integration of RNA-seq with RAD21 ChIP-Seq data analysis. Differential mRNA rank was compared to differential ChIP-Seq ranks in TSS (C) or whole gene regions (D). Ranks were calculated by signed $-\log_{10}$ as determined by edgeR (Ranked from most significant decrease to the most significant increase for: mRNA (x axis) vs ChIP signal (y axis)). Rank order bins of 1000 mRNA contigs each were generated. For each bin, the median (thick line) and interquartile range (gray area) are shown for the matched differential ChIP-Seq ranks (Spearman rank: $P = 9.35e{-}17$ (C), $P = 5.88e{-}12$ (D)). (**E**) Pathway analysis generated from RNA-seq and RAD21 ChIP-seq integration data. Enrichment analysis consists of matching gene IDs of possible targets for the 'common' and 'unique' sets with gene IDs in functional ontologies in MetaCore. The probability of a random intersection between a set of IDs the size of the target list with ontology entities is estimated by the $P$-value of the hypergeometric intersection. Data was generated using the Thompson Reuter MetaCore analysis GeneGo. Five pathways of the 10 most significant pathway maps are shown. The $\log_{10}$ of the $P$-value is presented (**F**). Validation of RNA-seq by qRT-PCR for specific genes in HCV infected cells normalized to non-infected cells. Differential expression was calculated using the equation of $2^{(-\Delta\Delta Ct)}$, with the GAPDH as endogenous controls. For RNA-seq and mRNA validation by qPCR six biological replicates were performed. (**G**) Validation of RAD21 ChIP-seq by qRT-PCR for specific genes in HCV infected cells normalized to non-infected cells. Differential expression was calculated using the equation of $2^{(-\Delta\Delta Ct)}$, with the GAPDH as an endogenous control. For ChIP-seq and ChIP-qPCR validation, five biological replicates were conducted. Values were normalized relative to qPCR for these genes following ChIP with normal Rabbit IgG Ab as control. (**H**) Validation of RAD21 ChIP-seq by qRT-PCR for specific genes in HCV infected cells normalized to non-infected cells, compared to HCV-cured cells following treatment with DAA normalized to non-infected cells treated with DAA. Differential expression was calculated using the equation of $2^{(-\Delta\Delta Ct)}$, with the GAPDH as an endogenous control. Values were normalized relative to qPCR for these genes following ChIP with normal Rabbit IgG Ab as control. Presented are means fold change compared to control ± SD from three independent experiments

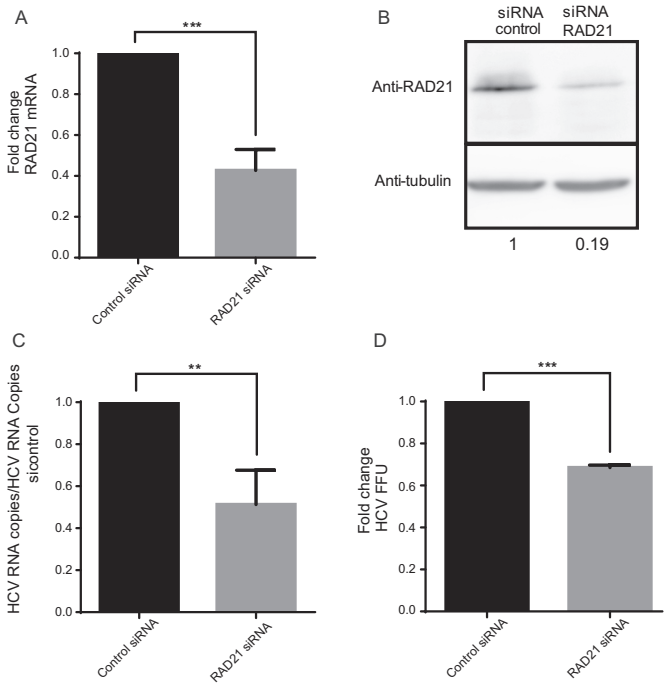


**Figure 3.** RAD21 level affects the efficiency of HCV infection. (**A**) Cells were transfected with RAD21 siRNA or control siRNA and infected with HJ3-5 chimeric virus at a MOI of 0.5. 48 hours following infection the cells were harvested for evaluation of the RAD21 RNA levels by qPCR as described above. (**B**) RAD21 protein level was evaluated by Western Blot. Protein levels were quantified and normalized to tubulin using the ImageJ software. (**C**) Level of HCV RNA was evaluated by qPCR. HCV RNA copies are calculated compared to non-infected Huh7.5 cells per ng of total cellular RNA. (**D**) Medium was collected to determine viral titer by FFU assay as previously described (31). Three biological replicates were performed for the experiment presented in A–D.

This dataset includes gene expression profiles of liver biopsies and clinical data from 216 patients with hepatitis C-related Child-Pugh class A cirrhosis. The log-rank test and Cox regression modeling were used to evaluate association between RAD21 expression and time from the enrollment to development of HCC. Patient samples were split into high and low RAD21 expressing groups based upon Z-score cutoff of 1 (Figure 5A). The results demonstrate more than twofold acceleration in HCC development (HR, 2.38; CI, 1.36–4.17; *P*-value = 0.0017) in HCV infected patients with high RAD21 expression compared to low RAD21 expression (Figure 5B). This dramatic difference in HCC development is obtained by only a minor change in RAD21 expression (high group *Z*-score: mean = 1.62, median = 1.48; low group *Z*-score: mean = –0.31, median = –0.26) (Figure 5A), implying that the 1.5–2-fold change in RAD21 expression we observed *in vitro* may have important implications for HCC development.

An intriguing hypothesis is that the viral-induced changes in cohesin binding may be associated with viral-induced CIN. We explored this possibility by comparing the RAD21 binding sites that are altered following HCV-infection that we have identified with a series of genomic intervals that encompass the boundaries of common copy number variations (CNVs) in HCC (generated by GISTIC2 algorithm) (43). Of 144 reported frequently aberrant CNV sites in HCC genomes, 34 sites overlapped with RAD21 binding sites. The difference between the expected random overlap among cohesin genomic positioning and CNV boundaries was calculated using INRICH algorithm (44) to be $1.16 \times 10^{-12}$. The significant level of overlap, considering that random steps would still be involved in determining the exact position of the CNV boundary, suggests a role for the cohesin positioning in the genome in the process that leads to CNVs in HCC. Moreover, the list of genes associated with cohesin binding site that are changes in HCV infected cells was compared with a another list of 98 genes within intervals of CNVs detected in HCC (45). Interestingly, 84 genes were common. The hypergeometric probability of this results is $P(X = 84) = 7.9 \times 10^{-31}$, validating the strong statistical correlation between cohesin binding sites and CNV events in HCC (Figure 5C).

### The chromosome abnormalities in mitotic cells are induced by the viral protein NS3 protease

The HCV proteins core and NS3 protease, were identified previously as those mainly responsible for the induction of chromosomal abnormalities in infected cells (5–8). Therefore, to dissect the mechanism by which HCV affects cohesin activity we transiently transfected Huh7.5 cells with each these viral genes: core, NS3/4A protease, or a control irrelevant protein (225, an anti-EGFR scFv (57)). Transfection efficiency was evaluated by immunostaining for the detection of transfected proteins, and was estimated as ∼50%. Cells were harvested 2 days post transfection, and the expression of *RAD21* was measured by qPCR. Transfection of core had no effect on the expression of RAD21. However, overexpression of NS3/4A induced a 1.5-fold increase in *RAD21* expression (Figure 6A).

If NS3/4A overexpression is sufficient to alter RAD21 expression, it may also be sufficient to induce hyper condensation of mitotic chromosomes and multispindles. To test this possibility, we arrested Huh7.5 cells that express an irrelevant control protein (scFv) or the viral protein core, as well as cells expressing NS3/4A in prometaphase by nocodazole 2 days post transfection. Chromosome spreads from these cells were immunostained to detect the spindle as described above (Figure 4). Remarkably, nuclei of cells that expressed NS3 alone revealed hypercondensed chromosomes in 50% of the cells, while this phenotype was observed in only about 10% of cells that expressed either core or a control protein (Figure 6B, C). Similarly, we observed that NS3/4A expression significantly increased the frequency of multi-spindle formation (Figure 6D and E).

The Huh7.5 cells respond to the overexpression of NS3/4A included increased levels of RAD21 expression, mitotic chromosome hypercondensation and increased frequency of multicentrosomes. This cell line is originated from hepatocellular carcinoma. We therefore, verified our results in the normal, immortalized human liver cell line THLE-3 (Figure 6F–H). These cells were previously used as normal liver cells control for HCC-derived cell lines (58–61). The THLE-3 cells were transfected with NS3/4A and transfection efficiency was determined by immunofluorescence as ∼40%. The effect of NS3/4A overexpression in

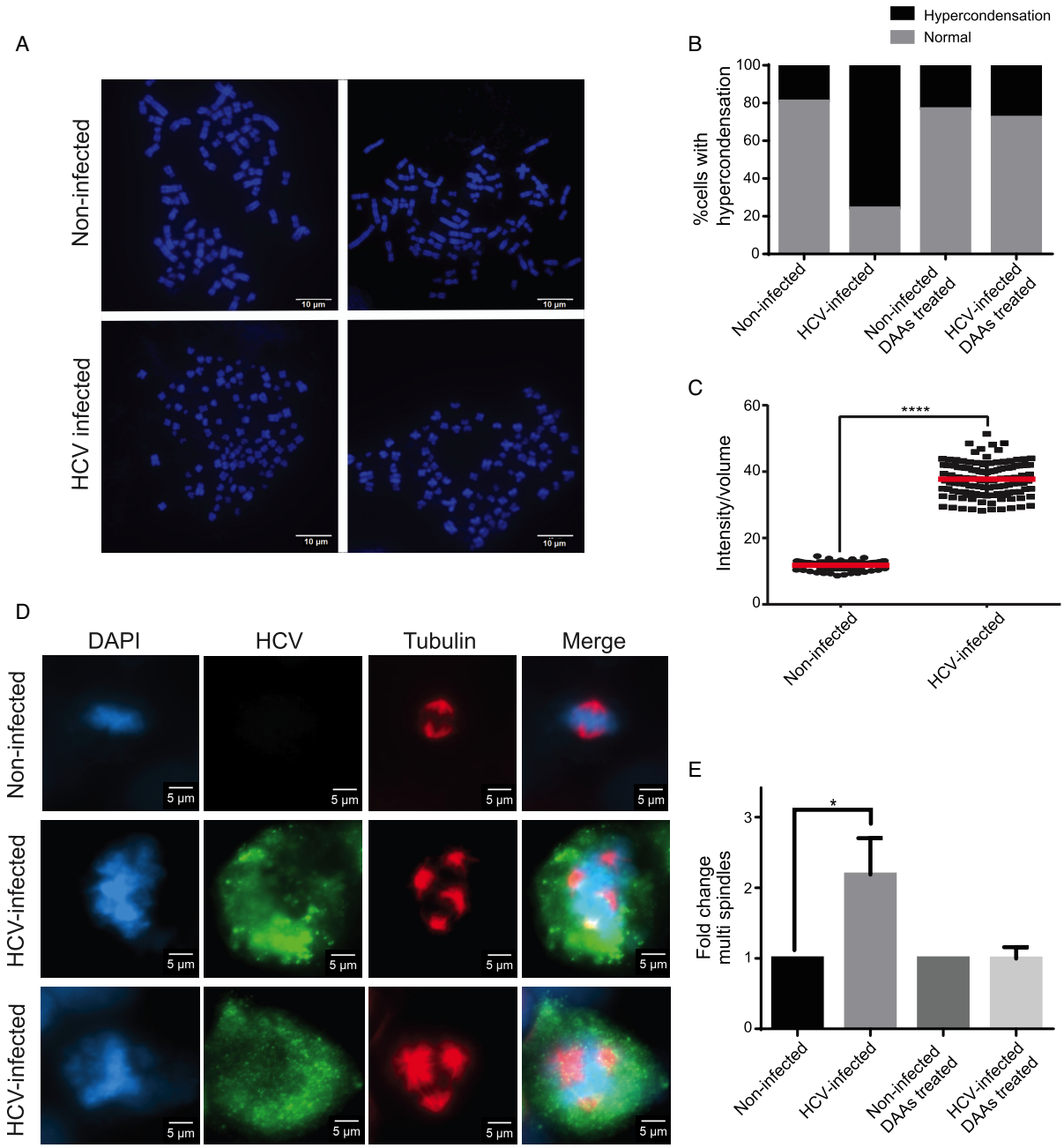


**Figure 4.** HCV infection induces chromosome hypercondensation and multipolar spindles in hepatoma cells. (**A**) HCV-infected (100% infected, generated as described in the methods) and non-infected Huh7.5 cells were treated with nocodazole. Chromosome spreads were prepared and stained with DAPI. Two representing images are shown for each condition. Scale Bar, 10 μm. (**B**) Non-infected, HCV-infected, non-infected DAA treated and HCV-cured cells following treatment with DAA were treated with nocodazole. Chromosome spreads were prepared and stained with DAPI. Chromosomes of each nucleus were defined as normal or hypercondensed according to their average length. Chromosomes were defined as hypercondensed if at least 2-fold decreased average length was measured compared to average length of chromosomes from nuclei of non-infected cells ($n = 300$). (**C**) Images of DAPI stained nuclei of infected and uninfected cells were imaged in three dimensions and deconvolved with Huygens Essential (Scientific Volume Imaging). The ratio between intensity to volume was measured for every chromosome separately by using Imaris (Bitplane) (****$P < 0.0001$, $t$-test). Red lines represent the median. (**D**) HCV infected and non-infected Huh7.5 cells were arrested in prometaphase by nocodazole. After synchronization, cells were immunostained. Representing images of non-infected (upper row) and HCV infected (middle and bottom rows) prometaphase cells immunostained for DNA (blue, DAPI), HCV with serum from HCV-infected patient (green, 488 Alexa fluor) and α-tubulin (yellow, Cy-3). Scale Bar, 5 μm. (**E**) Cells from non-infected, HCV-infected, non-infected-DAA treated and HCV-cured cells following treatment with DAA were stained with DAPI, anti HCV serum and anti-tubulin antibodies. Cells with two spindles were defined as normal, while three or more spindles were classified as cells with multipolar spindle. The fold change of nuclei containing multi spindles was calculated compared to control non infected cells and presented as means ± SD from three independent experiments. ($n = 219$-HCV infected, $n = 568$-non-infected, $n = 1183$-non-infected DAA treated and $n = 774$-HCV-cured DAA treated; *$P < 0.05$, $t$-test).

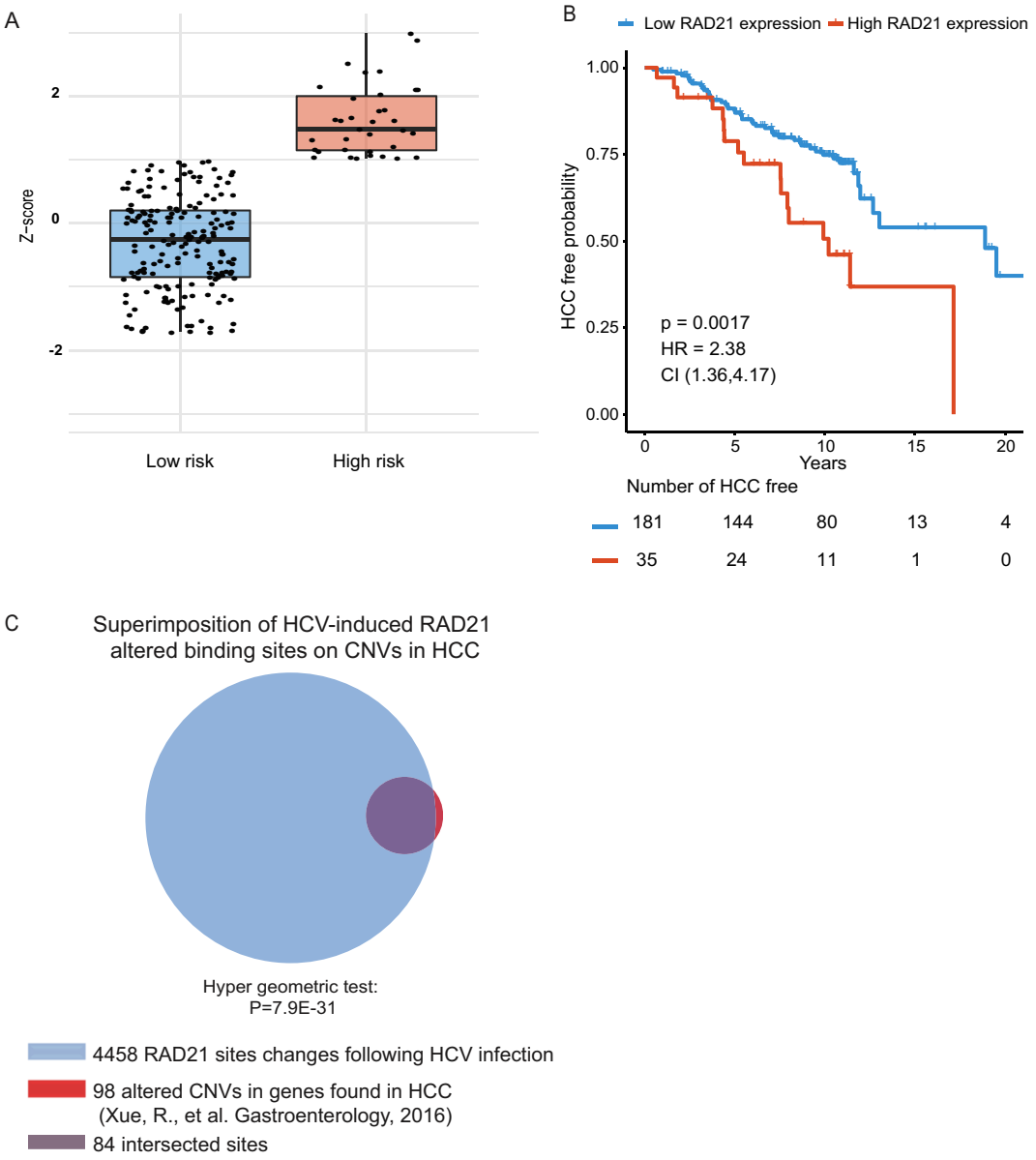


**Figure 5.** HCV-induced over expression of RAD21 is associated with HCC development. (**A**) Hepatitis C-related early stage cirrhosis samples (n = 216) were stratified into high ($n = 35$) and low risk ($n = 181$) groups based on *RAD21* expression levels (Z-score cutoff of 1). (**B**) Kaplan–Meier curves are shown for HCC development from the time of enrollment. *P*-value was calculated using log-rank test. The hazard ratio (HR) and 95% confidence interval are shown. (**C**) Superimposition of HCV-induced RAD21 binding sites on CNVs in HCC. Intersect between the list of genes associated with cohesin binding site that are changes in HCV infected cells with a list of 98 genes within intervals of CNVs detected in HCC (45). Eighty four genes were common. The hypergeometric probability of this results is $P(X = 84) = 7.9 \times 10^{-31}$.

THLE-3 cells was consistent with our previous results in Huh7.5 cells, indicating that it is a direct consequence of the viral protein and not related to the genetic background of the cells. This observation, combined with the rescue of hyper condensation phenotype we observed in cells treated with protease inhibitor (Figure 4B) suggest that NS3/4A is sufficient to induce hypercondensation, and that its catalytic protease activity is essential for this function.

Previous reports showed that WAPL depletion from cells inhibits cohesin dissolution and induces chromosome hypercondensation (22,23). Hence, we speculated that the hyper condensation of cohesin in HCV infected cells and NS3/4A over expressing cells may result from decreased levels of WAPL. We did not observe significant change in WAPL mRNA expression following HCV infection in the RNA-seq data (fold change = 1.12, Adjusted *P*-value = 0.0004). To test the possibility that levels of WAPL protein is decreased following HCV infection, we analyzed total protein extracts from uninfected and HCV-infected cells by western blot with antibody against WAPL. Strikingly, WAPL protein levels were approximately 80% lower in infected cells than in the non-infected control (Figure 6I).

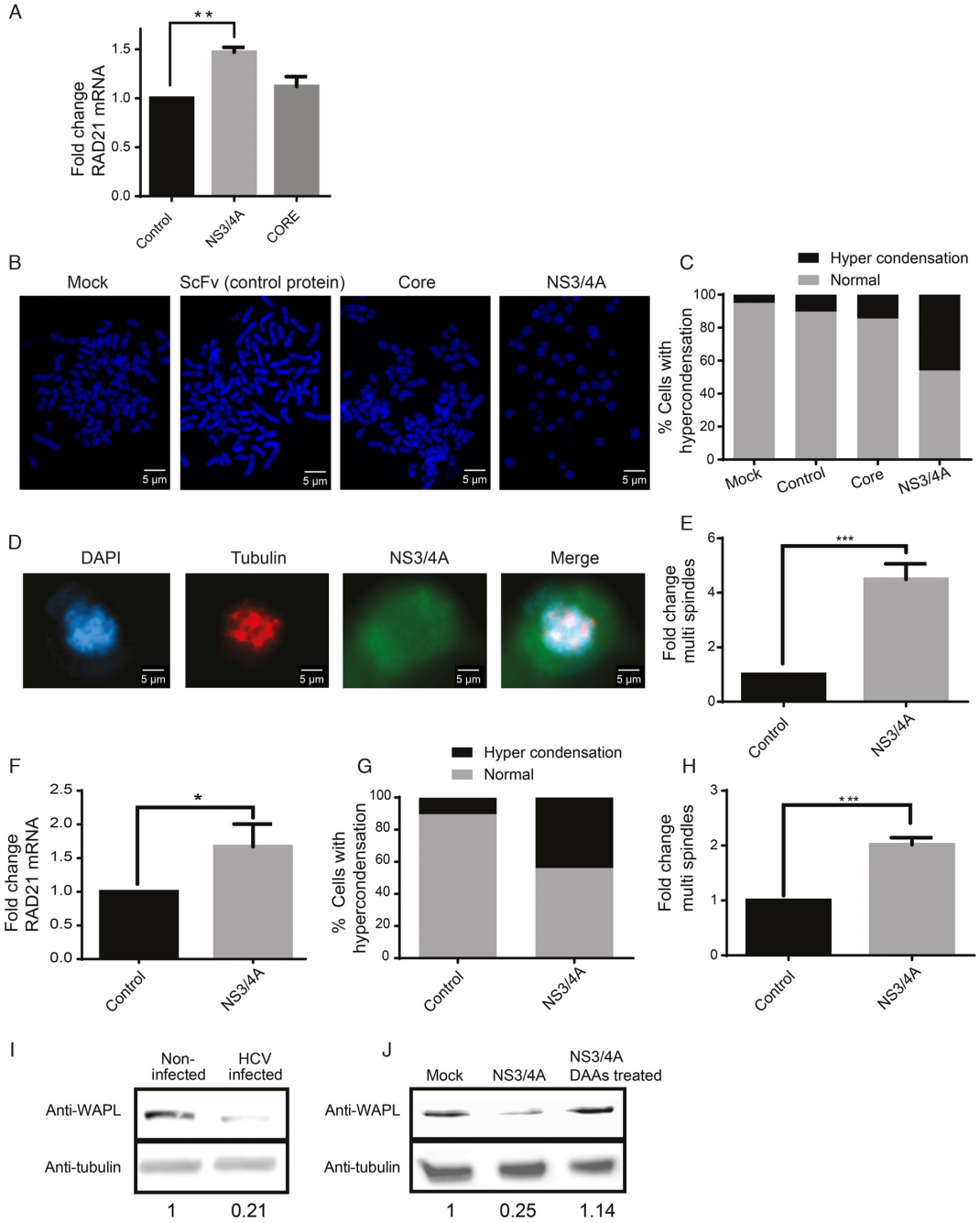


**Figure 6.** Overexpression of HCV protein NS3/4A induces chromosome abnormalities in hepatoma cells. (**A**) Huh7.5 cells transfected with plasmids for expression of control irrelevant protein (scFv), HCV NS3/4A or Core. Means mRNA levels of *RAD21* gene are shown ± SD from three independent experiments (**$P = 0.0064$, *t*-test). (**B**) Transfected cells were treated with nocodazole. Chromosome spreads were prepared and stained with DAPI. Representing chromosome images for each transfection are shown. Scale Bar, 5 µm. (**C**) Nuclei of each sample were defined as normal or small chromosomes according to their average length ($n = 150$). (**D**) NS3/4A transfected Huh7.5 cells were arrested in prometaphase by nocodazole. After synchronization, cells were immunostained. Representing image of transfected prometaphase cells immunostained for α-tubulin (yellow, Cy-3), DNA (blue, DAPI) and NS3 (green, alexa flour 488) are shown. Scale bar, 5 µm. (**E**) Nuclei of each sample were defined as normal or containing multipolar spindles ($n = 171$ (NS3 transfected) and 758 (mock transfected)). Means of fold change of nuclei with multi spindles compared to non-infected cells ± SD from three independent experiments are shown (*$P < 0.01$, *t*-test). (**F**) Normal human liver THLE-3 cells transfected with plasmid for expression of HCV NS3/4A. Means of mRNA levels of *RAD21* gene from three independent experiments are shown (*$P < 0.01$, *t*-test). (**G**) NS3/4A transfected THLE-3 cells were treated with nocodazole. Chromosome spreads were prepared and stained with DAPI. Nuclei of each sample were defined as normal or small chromosomes according to their average length ($n = 55$ (NS3 transfected) and 60 (mock transfected)). (**H**) NS3/4A transfected THLE-3 cells were arrested in prometaphase by nocodazole. After synchronization, cells were immunostained. Nuclei of each sample were defined as normal or containing multipolar spindles ($n = 166$ (NS3 transfected) and 280 (mock transfected)) Means of fold change of nuclei with multi spindles compared to non-infected cells ± SD from three independent experiments are shown (***$P < 0.0001$, *t*-test). (**I**) WAPL protein level in HCV-infected compared to non-infected cells was evaluated by Western Blot. Protein levels were quantified and normalized to tubulin using the ImageJ software. (**J**) WAPL protein level in control (empty vector) transfected cells, NS3/4A transfected cells and NS3/4A transfected cells following treatment with DAA was evaluated by Western Blot. Protein levels were quantified and normalized to tubulin using the ImageJ software.

Expression of NS3/4A in Huh7.5 cells was sufficient for decrease of WAPL level (Figure 6J). Furthermore, treating the NS3/4A transfected cells with NS3/4A inhibitor paritaprevir restored the WAPL to its levels in uninfected cells. These results support a mechanism whereby HCV induces chromosomal instability by decreasing the level of WAPL by NS3 protease activity, which in turn, inhibits cohesin dissociation from the chromosome.

## DISCUSSION

Cohesin is a major factor in the spatial organization of the genome. Misregulation of cohesin affects both gene expression and genome stability and may contribute to cell transformation. In this study, we show that an exclusively cytoplasmic virus, HCV, dysregulates cohesin and induces global alterations in chromatin structure and dynamics. We further demonstrate possible mechanisms by which the interplay between HCV and cohesin affects theses cellular processes and may contributes to the development of hepatocellular carcinoma (HCC).

Transcription is intimately controlled by the higher-order structure of chromatin that is being mediated by cohesin. Interphase chromatin is organized by Topological Associate Domains (TADs) that are formed by cohesin and CTCF. The current model for TAD formation includes extrusion of the DNA by cohesin which is paused by cohesin–CTCF interaction which is mediated by WAPL. TADs can be localized in either the gene expression active or inactive compartment (51). In addition, cohesin organizes the chromatin in TADs by creating chromatin loops that encourage interactions between distal enhancers and gene promoters. A common mechanism used by viruses is hijacking the cellular transcriptional machinery and enslaving it for the expression of genes and cellular pathways that are important for viral propagation (28). Our results strongly suggest that viral prevailing of the transcription machinery in infected cells may include alternations in the higher order structure of chromatin. We found that RAD21 is overexpressed in HCV infected cells and relocalized to new genomic loci. Increased levels of RAD21 may result in increased levels of assembled cohesin or change its cellular isoform ratio, for example the ratio of SA1 and SA2-containing complexes (62). Imbalance in the ratio of the cohesin core subunit SMC1 and SMC3 has been shown to affect the cohesin activity (63–66). The increased levels of RAD21 and its redistribution on chromosomes may affect transcription by mediating changes in the 3D organization that may lead to relocalization of TADs between compartments or affect intra-TADs organization. These changes will affect gene expression by both activation and suppression of genes. In agreement with this idea, we showed that cohesin is enriched in regulatory elements of genes associated with pathways that have been identified to be important for HCV life cycle. For example, one of the most significant pathway we identified to be altered in both RNA levels and RAD21 binding sites is regulation of lipid metabolism (Figure 2E). It is known that the virus misregulates the metabolism of lipids, an essential component for all steps of the HCV lifecycle, in the infected hepatocytes, which may lead to pathogenesis and cancer (28,67).

In addition to its role in gene expression regulation, cohesin is a key factor in maintaining genome stability. We showed that chromosomal instability induced by HCV includes multi-centrosomes and hypercondensation of mitotic chromosomes. Normal bipolar mitosis requires cohesin, and dysregulation of cohesin was associated with a multi-spindle phenotype (56,68). Expression of RAD21 mutant that cannot be cleaved by separase (68) or overexpression of SMC1 was shown to result in multi spindle mitosis and aneuploidy (69). The second observation related to alterations in chromatin structure in HCV infected cells is hypercondensation of mitotic chromosomes. The effect of hypercondensation on the stability of the genome is poorly understood. Hypercondensation has been reported in WAPL depleted cells, as well as in mutated NCAPD3 subunits of the SMC complex condensin II (70). However, the mechanism by which hyper condensation is induced is currently unclear.

Overexpression of RAD21 and downregulation of WAPL provide a strong foundation for dissecting the mechanism by which HCV regulates cohesin. We first showed that infection induces RAD21 overexpression, through acetylation of its promoter by HAT p300/CBP, which plays a role in viral infection. We further demonstrated that the level of the cohesin regulator WAPL is reduced in HCV-infected cells and correlated with expression of the viral NS3/4A protease. It has been suggested that WAPL restricts the size of TADs, and WAPL depletion results in increased loop size and hypercondensation (23,71). In addition, WAPL is a cohesin unloader and its depletion inhibits cohesin removal from the chromatin during in late G2 phase of the cell cycle (20). Cohesin residency at this stage may affect condensation by the condensin complex. Evidence on the interplay between cohesin and condensation has been described in model organisms (72–74). Recently, the role of WAPL in DNA repair has been described in yeast (75). The reduced levels of WAPL in HCV infected cells may contribute to the increased CIN through this mechanism. Prolonged association of cohesin with the chromosome as a result of WAPL removal may provide a mechanistic explanation for the observed G2/M cell cycle delay previously observed in HCV infected cells (4).

The identity of the viral protein involved in cohesin regulation is of great interest. We identified NS3/4A, a viral cysteine protease with both viral and cellular targets as the essential factor for WAPL downregulation (14). One possibility is that WAPL is a direct target of NS3/4A. Interestingly, we identified a NS3/4A cleavage site motif (D, E)XXXX(C,T)|(CA) in WAPL at position 955–961 (14). In future study we aim to determine if WAPL downregulation is mediated directly by NS3/4A and identify a direct interaction between NS3/4A and WAPL. A fundamental question to be addressed is the timing of NS3/4A-WAPL interaction. If NS3/4A is transported to the cell nuclease the interaction can occur throughout the cell cycle. Several reports suggest that NS3/4A is present in the nucleus during interphase (76–78). However, this reports used recombinant proteins and it is not yet clear if this localization also occur in HCV infected cells. Alternatively, cytoplasmic NS3/4A may gain access to the chromatin at prometaphase after nuclear envelope breakdown and chromatin condensation is

completed. The structure and functions of the NS3/4A protease are highly conserved between HCV and other members of the *Flaviviridae* virus family, such as flaviviruses, and thus, similar phenotypes may be induced by a broad range of viruses. In any case, the direct link between the viral protease and the cellular phenotype provides a novel mechanism by which HCV affects the host cell.

Chronic HCV infection of hepatoma cells is the leading cause of hepatocellular carcinoma (HCC). In recent years, the role of cohesin in cancer development has been established (79,80). Overexpression of RAD21 is associated with cell transformation (63–66,81,82). Overexpression of RAD21 may act similarly in HCV-infected cells and act as a driver of HCC. Here we demonstrate correlation between RAD21 expression levels, and the survival of HCC patients (Figure 5). The mechanistic basis of this observation may lay in the known effect of cohesin on the expression of cancer-related genes. We show that lipid metabolism and other pathways such as HGF and K-RAS signaling, which are known as mitogenic and tumorigenic (67,83,84), are upregulated through RAD21 (Figure 2). Therefore, cohesin-dependent transcription misregulation may directly or indirectly result in the activation of cancer-related genes that may contribute to future development of HCV-induced HCC. Indeed, overexpression of cohesin has been associated with dysregulation of known cancer related genes including RUNX1, RUNX3 and MYC, and of estrogen responsive genes, and with poor prognosis and resistance to therapies in cancer (reviewed in (19), (85)).

Another intriguing association between HCV-induced cohesin misregulation and HCC may be related to the specific chromosome aberrations frequently detected during HCC development (86). A recent study found that WAPL plays an important role in the repair of S-phase induced DNA breaks (74). This study suggests that WAPL reduction increase the frequency of deletions that result from improper repair of collapsed replication forks. We tested the correlation between RAD21 binding sites in HCV infected cells with frequency of common genomic deletions (43). We observed correlation between RAD21 residency and boundaries (Figure 5B). This correlation, together with correlation of high expression of RAD21 with lower patient's survival we identified, imply that HCV-related changes in cohesin expression and localization may provide a new mechanism for HCC development in HCV-infected patients. In conclusion, we propose a novel mechanism of HCV-induced dysregulation of cohesin, that leads to altered host gene expression, chromatin hypercompaction, and rare events of CIN and polyploidy.

## DATA AVAILABILITY

The RNA-seq and ChIP-seq data generated during the current study have been deposited in GEO repository with accession code GSE103730.

## SUPPLEMENTARY DATA

Supplementary Data are available at NAR Online.

## ACKNOWLEDGEMENTS

We thank the members of the Onn and Gal-Tanamy laboratories for helpful discussion and their comments on the manuscript; Dr Eyla Maoz for her technical help with flow cytometry; Prof. Itai Benhar for providing the NS3 and Core expression vectors.

## FUNDING

Leona M. and Harry B. Helmsley Charitable Trust Grant [2012PG-ISL013 to M.G.T., I.O., I.H.]; Israel Cancer Association [20160120 to M.G.T.];, Israel Cancer Association [20170111 to I.O.]; Israel Science Foundation Grant [1099/16 to I.O.]. Funding for open access charge: Research grants.

*Conflict of interest statement.* None declared.

## REFERENCES

1. El-Serag,H.B. and Rudolph,K.L. (2007) Hepatocellular carcinoma: epidemiology and molecular carcinogenesis. *Gastroenterology*, **132**, 2557–2576.
2. Kiyosawa,K., Umemura,T., Ichijo,T., Matsumoto,A., Yoshizawa,K., Gad,A. and Tanaka,E. (2004) Hepatocellular carcinoma: recent trends in Japan. *Gastroenterology*, **127**, S17–S26.
3. Mitchell,J.K., Lemon,S.M. and McGivern,D.R. (2015) How do persistent infections with hepatitis C virus cause liver cancer? *Curr. Opin. Virol.*, **14**, 101–108.
4. Kannan,R.P., Hensley,L.L., Evers,L.E., Lemon,S.M. and McGivern,D.R. (2011) Hepatitis C virus infection causes cell cycle arrest at the level of initiation of mitosis. *J. Virol.*, **85**, 7989–8001.
5. Machida,K., McNamara,G., Cheng,K.T., Huang,J., Wang,C.H., Comai,L., Ou,J.H. and Lai,M.M. (2010) Hepatitis C virus inhibits DNA damage repair through reactive oxygen and nitrogen species and by interfering with the ATM-NBS1/Mre11/Rad50 DNA repair pathway in monocytes and hepatocytes. *J. Immunol.*, **185**, 6985–6998.
6. Machida,K., Cheng,K.T., Sung,V.M., Lee,K.J., Levine,A.M. and Lai,M.M. (2004) Hepatitis C virus infection activates the immunologic (type II) isoform of nitric oxide synthase and thereby enhances DNA damage and mutations of cellular genes. *J. Virol.*, **78**, 8835–8843.
7. Lai,C.K., Jeng,K.S., Machida,K., Cheng,Y.S. and Lai,M.M. (2008) Hepatitis C virus NS3/4A protein interacts with ATM, impairs DNA repair and enhances sensitivity to ionizing radiation. *Virology*, **370**, 295–309.
8. Machida,K., Cheng,K.T., Lai,C.K., Jeng,K.S., Sung,V.M. and Lai,M.M. (2006) Hepatitis C virus triggers mitochondrial permeability transition with production of reactive oxygen species, leading to DNA damage and STAT3 activation. *J. Virol.*, **80**, 7199–7207.
9. Moradpour,D., Penin,F. and Rice,C.M. (2007) Replication of hepatitis C virus. *Nat. Rev. Microbiol.*, **5**, 453–463.
10. Morikawa,K., Lange,C.M., Gouttenoire,J., Meylan,E., Brass,V., Penin,F. and Moradpour,D. (2011) Nonstructural protein 3–4A: the Swiss army knife of hepatitis C virus. *J. Viral Hepatitis*, **18**, 305–315.
11. Meylan,E., Curran,J., Hofmann,K., Moradpour,D., Binder,M., Bartenschlager,R. and Tschopp,J. (2005) Cardif is an adaptor protein in the RIG-I antiviral pathway and is targeted by hepatitis C virus. *Nature*, **437**, 1167–1172.
12. Li,K., Foy,E., Ferreon,J.C., Nakamura,M., Ferreon,A.C., Ikeda,M., Ray,S.C., Gale,M. Jr and Lemon,S.M. (2005) Immune evasion by hepatitis C virus NS3/4A protease-mediated cleavage of the Toll-like receptor 3 adaptor protein TRIF. *Proc. Natl. Acad. Sci. U.S.A.*, **102**, 2992–2997.
13. Kang,X., Chen,X., He,Y., Guo,D., Guo,L., Zhong,J. and Shu,H.B. (2013) DDB1 is a cellular substrate of NS3/4A protease and required for hepatitis C virus replication. *Virology*, **435**, 385–394.
14. Morikawa,K., Gouttenoire,J., Hernandez,C., Dao Thi,V.L., Tran,H.T., Lange,C.M., Dill,M.T., Heim,M.H., Donze,O., Penin,F. *et al.* (2014) Quantitative proteomics identifies the

membrane-associated peroxidase GPx8 as a cellular substrate of the hepatitis C virus NS3-4A protease. *Hepatology*, **59**, 423–433.
15. Lee,B.K. and Iyer,V.R. (2012) Genome-wide studies of CCCTC-binding factor (CTCF) and cohesin provide insight into chromatin structure and regulation. *The J. Biol. Chem.*, **287**, 30906–30913.
16. Merkenschlager,M. and Odom,D.T. (2013) CTCF and cohesin: linking gene regulatory elements with their targets. *Cell*, **152**, 1285–1297.
17. Uhlmann,F. (2016) SMC complexes: from DNA to chromosomes. *Nat. Rev. Mol. Cell Biol.*, **17**, 399–412.
18. Onn,I., Heidinger-Pauli,J.M., Guacci,V., Unal,E. and Koshland,D.E. (2008) Sister chromatid cohesion: a simple concept with a complex reality. *Annu. Rev. Cell Dev. Biol.*, **24**, 105–129.
19. Rhodes,J.M., McEwan,M. and Horsfield,J.A. (2011) Gene regulation by cohesin in cancer: is the ring an unexpected party to proliferation? *Mol. Cancer Res.: MCR*, **9**, 1587–1607.
20. Gandhi,R., Gillespie,P.J. and Hirano,T. (2006) Human Wapl is a cohesin-binding protein that promotes sister-chromatid resolution in mitotic prophase. *Curr. Biol.: CB*, **16**, 2406–2417.
21. Kueng,S., Hegemann,B., Peters,B.H., Lipp,J.J., Schleiffer,A., Mechtler,K. and Peters,J.M. (2006) Wapl controls the dynamic association of cohesin with chromatin. *Cell*, **127**, 955–967.
22. Tedeschi,A., Wutz,G., Huet,S., Jaritz,M., Wuensche,A., Schirghuber,E., Davidson,I.F., Tang,W., Cisneros,D.A., Bhaskara,V. *et al.* (2013) Wapl is an essential regulator of chromatin structure and chromosome segregation. *Nature*, **501**, 564–568.
23. Haarhuis,J.H.I., van der Weide,R.H., Blomen,V.A., Yanez-Cuna,J.O., Amendola,M., van Ruiten,M.S., Krijger,P.H.L., Teunissen,H., Medema,R.H., van Steensel,B. *et al.* (2017) The cohesin release factor WAPL restricts chromatin loop extension. *Cell*, **169**, 693–707.
24. Busslinger,G.A., Stocsits,R.R., van der Lelij,P., Axelsson,E., Tedeschi,A., Galjart,N. and Peters,J.M. (2017) Cohesin is positioned in mammalian genomes by transcription, CTCF and Wapl. *Nature*, **544**, 503–507.
25. Arvey,A., Tempera,I., Tsai,K., Chen,H.S., Tikhmyanova,N., Klichinsky,M., Leslie,C. and Lieberman,P.M. (2012) An atlas of the Epstein-Barr virus transcriptome and epigenome reveals host–virus regulatory interactions. *Cell Host Microbe*, **12**, 233–245.
26. Kang,H., Wiedmer,A., Yuan,Y., Robertson,E. and Lieberman,P.M. (2011) Coordination of KSHV latent and lytic gene control by CTCF-cohesin mediated chromosome conformation. *PLoS Pathogens*, **7**, e1002140.
27. Lara-Pezzi,E., Pezzi,N., Prieto,I., Barthelemy,I., Carreiro,C., Martinez,A., Maldonado-Rodriguez,A., Lopez-Cabrera,M. and Barbero,J.L. (2004) Evidence of a transcriptional co-activator function of cohesin STAG/SA/Scc3. *J. Biol. Chem.*, **279**, 6553–6559.
28. Li,Q., Zhang,Y.Y., Chiu,S., Hu,Z., Lan,K.H., Cha,H., Sodroski,C., Zhang,F., Hsu,C.S., Thomas,E. *et al.* (2014) Integrative functional genomics of hepatitis C virus infection identifies host dependencies in complete viral replication cycle. *PLoS Pathogens*, **10**, e1004163.
29. Yi,M., Ma,Y., Yates,J. and Lemon,S.M. (2007) Compensatory mutations in E1, p7, NS2, and NS3 enhance yields of cell culture-infectious intergenotypic chimeric hepatitis C virus. *J. Virol.*, **81**, 629–638.
30. Podevin,P., Carpentier,A., Pene,V., Aoudjehane,L., Carriere,M., Zaidi,S., Hernandez,C., Calle,V., Meritet,J.F., Scatton,O. *et al.* (2010) Production of infectious hepatitis C virus in primary cultures of human adult hepatocytes. *Gastroenterology*, **139**, 1355–1364.
31. Gal-Tanamy,M., Zemel,R., Bachmatov,L., Jangra,R.K., Shapira,A., Villanueva,R.A., Yi,M., Lemon,S.M., Benhar,I. and Tur-Kaspa,R. (2010) Inhibition of protease-inhibitor-resistant hepatitis C virus replicons and infectious virus by intracellular intrabodies. *Antiviral Res.*, **88**, 95–106.
32. El-Shamy,A., Eng,F.J., Doyle,E.H., Klepper,A.L., Sun,X., Sangiovanni,A., Iavarone,M., Colombo,M., Schwartz,R.E., Hoshida,Y. *et al.* (2015) A cell culture system for distinguishing hepatitis C viruses with and without liver cancer-related mutations in the viral core gene. *J. Hepatol.*, **63**, 1323–1333.
33. Steenbergen,R.H., Joyce,M.A., Thomas,B.S., Jones,D., Law,J., Russell,R., Houghton,M. and Tyrrell,D.L. (2013) Human serum leads to differentiation of human hepatoma cells, restoration of very-low-density lipoprotein secretion, and a 1000-fold increase in HCV Japanese fulminant hepatitis type 1 titers. *Hepatology*, **58**, 1907–1917.
34. Bose,S.K., Meyer,K., Di Bisceglie,A.M., Ray,R.B. and Ray,R. (2012) Hepatitis C virus induces epithelial-mesenchymal transition in primary human hepatocytes. *J. Virol.*, **86**, 13621–13628.
35. Li,H. and Durbin,R. (2009) Fast and accurate short read alignment with Burrows-Wheeler transform. *Bioinformatics*, **25**, 1754–1760.
36. Dobin,A., Davis,C.A., Schlesinger,F., Drenkow,J., Zaleski,C., Jha,S., Batut,P., Chaisson,M. and Gingeras,T.R. (2013) STAR: ultrafast universal RNA-seq aligner. *Bioinformatics*, **29**, 15–21.
37. Quinlan,A.R. and Hall,I.M. (2010) BEDTools: a flexible suite of utilities for comparing genomic features. *Bioinformatics*, **26**, 841–842.
38. Robinson,M.D., McCarthy,D.J. and Smyth,G.K. (2010) edgeR: a Bioconductor package for differential expression analysis of digital gene expression data. *Bioinformatics*, **26**, 139–140.
39. Liao,Y., Smyth,G.K. and Shi,W. (2014) featureCounts: an efficient general purpose program for assigning sequence reads to genomic features. *Bioinformatics*, **30**, 923–930.
40. Bessarabova,M., Ishkin,A., JeBailey,L., Nikolskaya,T. and Nikolsky,Y. (2012) Knowledge-based analysis of proteomics data. *BMC Bioinformatics*, **13**(Suppl. 16), S13.
41. Andrews,N.C. and Faller,D.V. (1991) A rapid micropreparation technique for extraction of DNA-binding proteins from limiting numbers of mammalian cells. *Nucleic Acids Res.*, **19**, 2499.
42. Hoshida,Y., Villanueva,A., Sangiovanni,A., Sole,M., Hur,C., Andersson,K.L., Chung,R.T., Gould,J., Kojima,K., Gupta,S. *et al.* (2013) Prognostic gene expression signature for patients with hepatitis C-related early-stage cirrhosis. *Gastroenterology*, **144**, 1024–1030.
43. Wang,K., Lim,H.Y., Shi,S., Lee,J., Deng,S., Xie,T., Zhu,Z., Wang,Y., Pocalyko,D., Yang,W.J. *et al.* (2013) Genomic landscape of copy number aberrations enables the identification of oncogenic drivers in hepatocellular carcinoma. *Hepatology*, **58**, 706–717.
44. Lee,P.H., O'Dushlaine,C., Thomas,B. and Purcell,S.M. (2012) INRICH: interval-based enrichment analysis for genome-wide association studies. *Bioinformatics*, **28**, 1797–1799.
45. Xue,R., Li,R., Guo,H., Guo,L., Su,Z., Ni,X., Qi,L., Zhang,T., Li,Q., Zhang,Z. *et al.* (2016) Variable intra-tumor genomic heterogeneity of multiple lesions in patients with hepatocellular carcinoma. *Gastroenterology*, **150**, 998–1008.
46. Faure,A.J., Schmidt,D., Watt,S., Schwalie,P.C., Wilson,M.D., Xu,H., Ramsay,R.G., Odom,D.T. and Flicek,P. (2012) Cohesin regulates tissue-specific expression by stabilizing highly occupied cis-regulatory modules. *Genome Res.*, **22**, 2163–2175.
47. Polak,P., Karlic,R., Koren,A., Thurman,R., Sandstrom,R., Lawrence,M.S., Reynolds,A., Rynes,E., Vlahovicek,K., Stamatoyannopoulos,J.A. *et al.* (2015) Cell-of-origin chromatin organization shapes the mutational landscape of cancer. *Nature*, **518**, 360–364.
48. Haqshenas,G., Wu,J., Simpson,K.J., Daly,R.J., Netter,H.J., Baumert,T.F. and Doerig,C. (2017) Signalome-wide assessment of host cell response to hepatitis C virus. *Nat. Commun.*, **8**, 15158.
49. Merkenschlager,M. and Nora,E.P. (2016) CTCF and cohesin in genome folding and transcriptional gene regulation. *Annu. Rev. Genomics Hum. Genet.*, **17**, 17–43.
50. Gibcus,J.H. and Dekker,J. (2013) The hierarchy of the 3D genome. *Mol. Cell*, **49**, 773–782.
51. Fortin,J.P. and Hansen,K.D. (2015) Reconstructing A/B compartments as revealed by Hi-C using long-range correlations in epigenetic data. *Genome Biol.*, **16**, 180.
52. Mehta,G.D., Rizvi,S.M. and Ghosh,S.K. (2012) Cohesin: a guardian of genome integrity. *Biochim. Biophys. Acta*, **1823**, 1324–1342.
53. Baek,K.H., Park,H.Y., Kang,C.M., Kim,S.J., Jeong,S.J., Hong,E.K., Park,J.W., Sung,Y.C., Suzuki,T., Kim,C.M. *et al.* (2006) Overexpression of hepatitis C virus NS5A protein induces chromosome instability via mitotic cell cycle dysregulation. *J. Mol. Biol.*, **359**, 22–34.
54. Machida,K., Liu,J.C., McNamara,G., Levine,A., Duan,L. and Lai,M.M. (2009) Hepatitis C virus causes uncoupling of mitotic checkpoint and chromosomal polyploidy through the Rb pathway. *J. Virol.*, **83**, 12590–12600.
55. Asselah,T., Boyer,N., Saadoun,D., Martinot-Peignoux,M. and Marcellin,P. (2016) Direct-acting antivirals for the treatment of hepatitis C virus infection: optimizing current IFN-free treatment and future perspectives. *Liver Int.*, **36**(Suppl. 1), 47–57.

56. Beauchene,N.A., Diaz-Martinez,L.A., Furniss,K., Hsu,W.S., Tsai,H.J., Chamberlain,C., Esponda,P., Gimenez-Abian,J.F. and Clarke,D.J. (2010) Rad21 is required for centrosome integrity in human cells independently of its role in chromosome cohesion. *Cell Cycle*, **9**, 1774–1780.
57. Beerli,R.R., Wels,W. and Hynes,N.E. (1994) Autocrine inhibition of the epidermal growth factor receptor by intracellular expression of a single-chain antibody. *Biochem. Biophys. Res. Commun.*, **204**, 666–672.
58. Ding,G., Liu,H.D., Huang,Q., Liang,H.X., Ding,Z.H., Liao,Z.J. and Huang,G. (2013) HDAC6 promotes hepatocellular carcinoma progression by inhibiting P53 transcriptional activity. *FEBS Lett.*, **587**, 880–886.
59. Pfeifer,A.M., Cole,K.E., Smoot,D.T., Weston,A., Groopman,J.D., Shields,P.G., Vignaud,J.M., Juillerat,M., Lipsky,M.M., Trump,B.F. *et al.* (1993) Simian virus 40 large tumor antigen-immortalized normal human liver epithelial cells express hepatocyte characteristics and metabolize chemical carcinogens. *Proc. Natl. Acad. Sci. U.S.A.*, **90**, 5123–5127.
60. Chan,C., Wang,Y., Chow,P.K., Chung,A.Y., Ooi,L.L. and Lee,C.G. (2013) Altered binding site selection of p53 transcription cassettes by hepatitis B virus X protein. *Mol. Cell. Biol.*, **33**, 485–497.
61. Quagliata,L., Matter,M.S., Piscuoglio,S., Arabi,L., Ruiz,C., Procino,A., Kovac,M., Moretti,F., Makowska,Z., Boldanova,T. *et al.* (2014) Long noncoding RNA HOTTIP/HOXA13 expression is associated with disease progression and predicts outcome in hepatocellular carcinoma patients. *Hepatology*, **59**, 911–923.
62. Sumara,I., Vorlaufer,E., Gieffers,C., Peters,B.H. and Peters,J.M. (2000) Characterization of vertebrate cohesin complexes and their regulation in prophase. *J. Cell Biol.*, **151**, 749–762.
63. Laugsch,M., Seebach,J., Schnittler,H. and Jessberger,R. (2013) Imbalance of SMC1 and SMC3 cohesins causes specific and distinct effects. *PLoS One*, **8**, e65149.
64. Deb,S., Xu,H., Tuynman,J., George,J., Yan,Y., Li,J., Ward,R.L., Mortensen,N., Hawkins,N.J., McKay,M.J. *et al.* (2014) RAD21 cohesin overexpression is a prognostic and predictive marker exacerbating poor prognosis in KRAS mutant colorectal carcinomas. *Br. J. Cancer*, **110**, 1606–1613.
65. Davis,S.J., Sheppard,K.E., Anglesio,M.S., George,J., Traficante,N., Fereday,S., Intermaggio,M.P., Menon,U., Gentry-Maharaj,A., Lubinski,J. *et al.* (2015) Enhanced GAB2 expression is associated with improved survival in High-Grade serous ovarian cancer and sensitivity to PI3K inhibition. *Mol. Cancer Ther.*, **14**, 1495–1503.
66. Bernardes,V.F., Correa,G.T., Loyola,A.M., Cardoso,S.V., de Paula,A.M., Cabral,M.M., Gomez,R.S. and Gomes,C.C. (2014) STAG2 expression in oral cancer and potentially malignant lesions. *Tumour Biol.*, **35**, 3641–3645.
67. Adinolfi,L.E., Rinaldi,L., Guerrera,B., Restivo,L., Marrone,A., Giordano,M. and Zampino,R. (2016) NAFLD and NASH in HCV Infection: Prevalence and Significance in Hepatic and Extrahepatic Manifestations. *Int. J. Mol. Sci.*, **17**, E803.
68. Diaz-Martinez,L.A., Beauchene,N.A., Furniss,K., Esponda,P., Gimenez-Abian,J.F. and Clarke,D.J. (2010) Cohesin is needed for bipolar mitosis in human cells. *Cell Cycle*, **9**, 1764–1773.
69. Wong,R.W. (2010) Interaction between Rae1 and cohesin subunit SMC1 is required for proper spindle formation. *Cell cycle*, **9**, 198–200.
70. Bakhrebah,M., Zhang,T., Mann,J.R., Kalitsis,P. and Hudson,D.F. (2015) Disruption of a conserved CAP-D3 threonine alters condensin loading on mitotic chromosomes leading to chromosome hypercondensation. *J. Biol. Chem.*, **290**, 6156–6167.
71. Wutz,G., Varnai,C., Nagasaka,K., Cisneros,D.A., Stocsits,R.R., Tang,W., Schoenfelder,S., Jessberger,G., Muhar,M., Hossain,M.J. *et al.* (2017) Topologically associating domains and chromatin loops depend on cohesin and are regulated by CTCF, WAPL, and PDS5 proteins. *EMBO J.*, **36**, 3573–3599.
72. Lavoie,B.D., Hogan,E. and Koshland,D. (2004) In vivo requirements for rDNA chromosome condensation reveal two cell-cycle-regulated pathways for mitotic chromosome folding. *Genes Dev.*, **18**, 76–87.
73. Orgil,O., Matityahu,A., Eng,T., Guacci,V., Koshland,D. and Onn,I. (2015) A conserved domain in the scc3 subunit of cohesin mediates the interaction with both mcd1 and the cohesin loader complex. *PLoS Genet.*, **11**, e1005036.
74. Bloom,M.S., Koshland,D. and Guacci,V. (2017) Cohesin function in cohesion, condensation and DNA repair is regulated by Wpl1p via a common mechanism in Saccharomyces cerevisiae. *Genetics*, **208**, 111–124.
75. Bloom,M.S., Koshland,D. and Guacci,V. (2018) Cohesin function in cohesion, condensation, and DNA repair is regulated by Wpl1p via a common mechanism in Saccharomyces cerevisiae. *Genetics*, **208**, 111–124.
76. Wolk,B., Sansonno,D., Krausslich,H.G., Dammacco,F., Rice,C.M., Blum,H.E. and Moradpour,D. (2000) Subcellular localization, stability, and trans-cleavage competence of the hepatitis C virus NS3-NS4A complex expressed in tetracycline-regulated cell lines. *J. Virol.*, **74**, 2293–2304.
77. Muramatsu,S., Ishido,S., Fujita,T., Itoh,M. and Hotta,H. (1997) Nuclear localization of the NS3 protein of hepatitis C virus and factors affecting the localization. *J. Virol.*, **71**, 4954–4961.
78. Levin,A., Neufeldt,C.J., Pang,D., Wilson,K., Loewen-Dobler,D., Joyce,M.A., Wozniak,R.W. and Tyrrell,D.L. (2014) Functional characterization of nuclear localization and export signals in hepatitis C virus proteins and their role in the membranous web. *PLoS One*, **9**, e114629.
79. Losada,A. (2014) Cohesin in cancer: chromosome segregation and beyond. *Nat. Rev. Cancer*, **14**, 389–393.
80. Watrin,E., Kaiser,F.J. and Wendt,K.S. (2016) Gene regulation and chromatin organization: relevance of cohesin mutations to human disease. *Curr. Opin. Genet. Dev.*, **37**, 59–66.
81. Yan,M., Xu,H., Waddell,N., Shield-Artin,K., Haviv,I., kConFab,a., McKay,M.J. and Fox,S.B. (2012) Enhanced RAD21 cohesin expression confers poor prognosis in BRCA2 and BRCAX, but not BRCA1 familial breast cancers. *Breast Cancer Res.: BCR*, **14**, R69.
82. Xu,H., Yan,M., Patra,J., Natrajan,R., Yan,Y., Swagemakers,S., Tomaszewski,J.M., Verschoor,S., Millar,E.K., van der Spek,P. *et al.* (2011) Enhanced RAD21 cohesin expression confers poor prognosis and resistance to chemotherapy in high grade luminal, basal and HER2 breast cancers. *Breast Cancer Res.: BCR*, **13**, R9.
83. Fajardo-Puerta,A.B., Mato Prado,M., Frampton,A.E. and Jiao,L.R. (2016) Gene of the month: HGF. *J. Clin. Pathol.*, **69**, 575–579.
84. Nussinov,R., Tsai,C.J., Muratcioglu,S., Jang,H., Gursoy,A. and Keskin,O. (2015) Principles of K-Ras effector organization and the role of oncogenic K-Ras in cancer initiation through G1 cell cycle deregulation. *Expert Rev. Proteomics*, **12**, 669–682.
85. Cohen-Zinder,M., Karasik,D. and Onn,I. (2013) Structural maintenance of chromosome complexes and bone development: the beginning of a wonderful relationship? *BoneKEy Rep.*, **2**, 388.
86. Lau,S.H. and Guan,X.Y. (2005) Cytogenetic and molecular genetic alterations in hepatocellular carcinoma. *Acta Pharmacol. Sinica*, **26**, 659–665.